CHEMICAL REVIEWS

Review

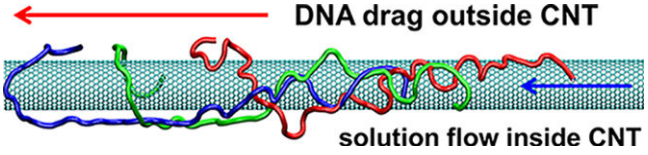
pubs.acs.org/CR

Material Drag Phenomena in Nanotubes

Petr Král*,†,‡ and Boyang Wang*,†,§

†Department of Chemistry, and ‡Department of Physics, University of Illinois at Chicago, Chicago, Illinois 60607, United States

§Institute of Chemistry, Chinese Academy of Sciences, Beijing 100190, People's Republic of China



CONTENTS

1. Introduction 3372
2. Material–Electron Drag in Nanotubes 3373
2.1. Material Drag Induced by Electron Flow 3373
2.2. Electron Drag Induced by Flowing Polar Liquids 3375
2.3. Electron Drag Induced by Flowing Gases 3376
3. Material Drag in Nanotubes Induced by Fluidic Flow 3377
3.1. Coulombic Drag of Molecules Induced by Distant Flow 3377
3.1.1. Dragging of Molecules on Nanotubes by Water Flowing through Their Interior 3377
3.1.2. Dragging of Nanodroplets on Nanotubes by Ions Passing through Their Interior 3378
3.1.3. Dragging of Solvated DNA on Nanotubes by Ionic Solutions Flowing through Their Interior 3380
3.1.4. Guided Self-Assembly of Filled Micelles on Nanotubes 3380
3.2. Electrokinetic Drag of Molecules 3381
3.2.1. Modeling of Electrokinetic Phenomena 3381
3.2.2. Electrophoretic Drag in Nanotubes 3381
3.2.3. Electroosmotic Drag in Nanotubes 3382
3.2.4. Other Fluidic Drag Mechanisms 3383
4. Material Drag in Nanotubes Induced by Mechanistic Means 3384
4.1. Thermal Gradient Drag of Molecular Assemblies 3384
4.2. Coherent Phonon Drag of Nanodroplets 3384
4.3. Chemically Tunable Nanoscale Liquid Propellers 3385
5. Conclusions 3386
Author Information 3386
Corresponding Author 3386
Notes 3386
Biographies 3386
Acknowledgments 3387
References 3387

1. INTRODUCTION

Biological systems continuously perform active molecular transport at the cellular level by using their individually developed highly sophisticated molecular machinery.[1] Motor proteins, such as kinesin,[2] myosin,[3] and dynein,[4] are capable of translating molecules and micelles along tubulous filaments, and provide motility to bacteria.[5] In their efforts to perform controlled manipulation of matter on a nanoscale, humans try to not only operate this molecular machinery in vitro,[6] but also to design biomimetically related synthetic systems.[7,8] Synthetic molecular machines may be capable of operating in special environments over a wide range of temperatures and at high speeds. Synthetic molecular motors[9] can provide linear[10] and rotary[11−15] motions, and be powered by chemical,[14] optical,[16−18] and mechanical means.[19] In the future, it may be that natural and synthetic systems will coevolve to acquire unprecedented abilities and functions.[20,21]

Carbon nanotubes (CNT) and boron−nitride nanotubes (BNT)[22−30] have many unique properties that have proven very useful for molecular transport, even at the cellular level.[31,32] Both single-wall (SWNT) and multiwall (MWNT) carbon nanotubes are very strong and chemically stable. In addition, they exhibit very low friction with themselves and other molecules.[33] They can be either conducting or semiconducting,[34] and be modified by physisorption[35,36] or by the covalent bonding of molecular ligands.[37] BNTs have large energy band gaps,[30] high oxidation resistivity, thermal and chemical stability,[38,39] and they possess piezoelectric properties.[40,41]

Soon after their discovery, CNTs were successfully intercalated with inorganic materials,[42] metals,[43−47] as well as other molecules.[49,48] For example, in Figure 1 an STM image of CNT filled with close packed C_{60} fullerenes (peapod) is presented.[48] It was proposed that individual C_{60} and carbon nanocapsules intercalated in CNTs could act as potential memory agents[50] and motors.[51] The hollow core and evident similarity of CNTs to biological tubulous filaments raised questions about the possible use of CNTs for atomic and molecular transport.[52]

In this Review, we will discuss transport methods that can be used to drag atoms and molecules into the interior and onto the external surfaces of carbon nanotubes. We hope to cover the current literature on molecular drag in nanotubes, cite the results of these studies, and discuss in more detail the most important and original contributions. The literature is less complete in the area of electrokinetic phenomena, which constitute a category of their own but are briefly discussed here

Received: July 1, 2011
Published: February 14, 2013

 © 2013 American Chemical Society dx.doi.org/10.1021/cr200244h | Chem. Rev. 2013, 113, 3372−3390

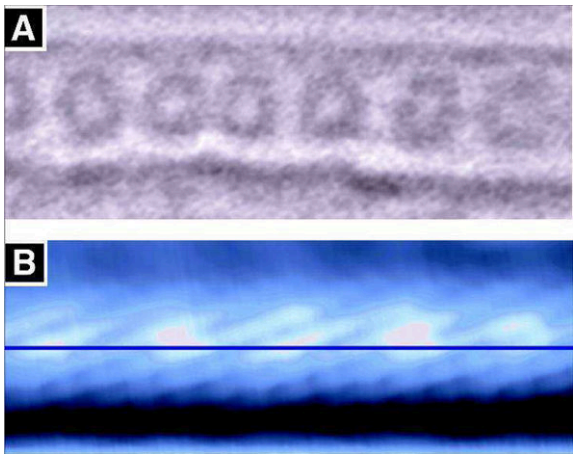


Figure 1. TEM and STM images of a CNT peapod. (A) A room temperature TEM image (105 × 29 Å^2) of a peapod, showing the SWNT cage and encapsulated C_{60} molecules. (B) STM image of a peapod obtained under positive sample bias, showing both atomic corrugation of the SWNT and features associated with the encapsulated C_{60} molecules. Reproduced with permission from ref 48. Copyright 2002 AAAS.

as as specific drag phenomena. The outline of this Review is as follows: In section II, we will review the dragging of atoms and molecules both inside and outside nanotubes by using electric currents passing through them. In addition, we will discuss the generation of such electronic currents by ions and molecules flowing around the nanotubes. In section III, we review the dragging of molecules by nanofluidic methods. We discuss their dragging by Coulombic scattering with separately flowing fluids, and outline electrokinetic phenomena in nanotubes. In section IV, we review the dragging of molecules along nanotubes by phonon flows generated in thermal gradients, by coherent acoustic waves, and by the mechanical propelling of functionalized nanotubes. Some general conclusions are presented in section V.

2. MATERIAL–ELECTRON DRAG IN NANOTUBES

Electrons, phonons, and other elementary excitations interact and drag each other when traveling in solid-state materials.[53] These drag phenomena are caused by a mutual transfer of momenta between the scattering elementary excitations present in the same medium. Similar drag phenomena are experimentally observed when elementary excitations couple at a distance. For example, electron drag was measured in a sandwiched nanostructure,[54] where the electrons moving in one δ-doped GaAs layer were separated by a ~20 nm thick nonconducting AlGaAs layer from the electrons dragged in another δ-doped GaAs layer. These observations were interpreted in two different ways. They were seen either as a consequence of direct electron–electron coupling of the electrons in the two δ-doped GaAs layers[55,56] or as a consequence of indirect electron coupling via the phonons present in the intermediate layer.[57]

In general, many drag phenomena can be interpreted as a specific type of ratchet,[58] which occurs in the presence of (1) asymmetric potentials on which particles can be dragged and (2) nonequilibrium fluctuations. Both conditions are essential for particle dragging. In an equilibrium, particles manifest thermally induced Brownian motion, which does not lead to drag even in the presence of asymmetric potentials. Similarly, if particles move on a symmetric potential, the presence of a general nonequilibrium is not a sufficient condition for their dragging.

2.1. Material Drag Induced by Electron Flow

In electromigration, charged atoms and molecules are dragged on material surfaces by external electric fields.[59−61] The particles are driven by the total force as expressed by the equation:

$$F_{tot} \approx F_d + F_w \quad (1)$$

where the direct force, F_d, is caused by the (locally modified) external electric field, and the wind force, F_w, is caused by scattering of conduction electrons on the atoms/molecules. Whereas in isolators (where there are no free electrons), the direct force usually dominates, these forces often cannot be unambiguously separated.

It was theoretically proposed[52] that, analogous to molecular transport mechanisms in biology,[2−4] atoms and molecules adsorbed onto CNTs or intercalated into their interior could be dragged by scattering electrons in electric currents. The electric currents could be generated by an external bias from two electrodes attached to the CNTs or by special optical excitations. In the coherent control method, schematically shown in Figure 2, simultaneous excitation of semiconducting

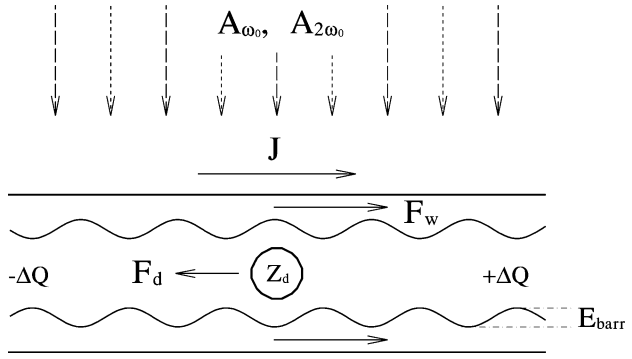


Figure 2. Functional scheme of a nanotube-based atomic pump. Combined laser excitation at frequencies ω_0 and $2\omega_0$, with beams polarized along the tube axis, induces a current J in the tube, which exerts the wind force F_w on an atom carrying the net charge Z_d. Reflected carriers build up charges $\pm\Delta Q$, which generate a local electric field causing a direct force F_d to act on the atom. The atomic motion in the tube occurs on a potential energy surface with activation barriers E_{barr}. Reproduced with permission from ref 52. Copyright 1999 American Physical Society.

CNTs by two laser beams with frequencies ω_0 and $2\omega_0$ can inject electrons with a nonzero momentum in their conduction band.[62−68] The direction of the current (electron momentum) can be controlled by the relative phase of the two laser beams, $\delta = \delta_{2\omega 0} - 2\delta_{\omega 0}$. Because no special crystal symmetry is required for this mechanism to work, the current can be generated in both isolated[69] and bundled[70] single-wall as well as multiwall CNTs.

The electric current can displace atoms intercalated inside the CNTs, as schematically depicted in Figure 2. One possibility is lithium atoms, which were experimentally intercalated into the CNTs with the goal of testing the modified CNTs in Li battery applications.[47] The motion of a partially charged Li atom (as a result of charge transfer to the CNT) is induced by exerting the wind force, F_w, on it

dx.doi.org/10.1021/cr200244h | Chem. Rev. 2013, 113, 3372–3390

(scattering of the injected electrons from the atom). In contrast, the direct force, F_d, caused by a local charge buildup, $\pm\Delta Q$, of electrons reflected from the atom, is much smaller.

The barriers, E_{barr}, associated with intersite hopping of the Li atom on the CNT surface are shifted by the total force acting on the atom, $F_{tot} = F_d + F_w$, over the distance of the lattice constant, l_t = 1.42 Å. Consequently, the atom hopping rates toward left and right are given by the following equation:

$$\gamma_{L,R} = \gamma_0 \exp\left(-\frac{E_{barr} \pm F_{tot} l_t}{k_B T}\right) \quad (2)$$

respectively, where $\gamma_0 = [(2E_{barr})/(m_{Li}\ l_t^2)]^{1/2}$ is the atomic vibration frequency for the Li atom, and m_{Li} is its atomic mass. For moderate driving, this yields the average atom drag velocity, as expressed in the equation:

$$\langle v_{at} \rangle = (\gamma_L - \gamma_R) l_t \approx \frac{2\gamma_0 F_{tot} l_t^2}{k_B T} \exp\left(-\frac{E_{barr}}{k_B T}\right) \approx 5\text{–}25 \text{ nm/}\mu\text{s} \quad (3)$$

It is strongly dependent on temperature T.[52]

The proposed drag of materials on CNT surfaces by electric currents was experimentally realized in a setup as demonstrated in Figure 3 (top).[71] Here, the dc electric current of ~40 μA was

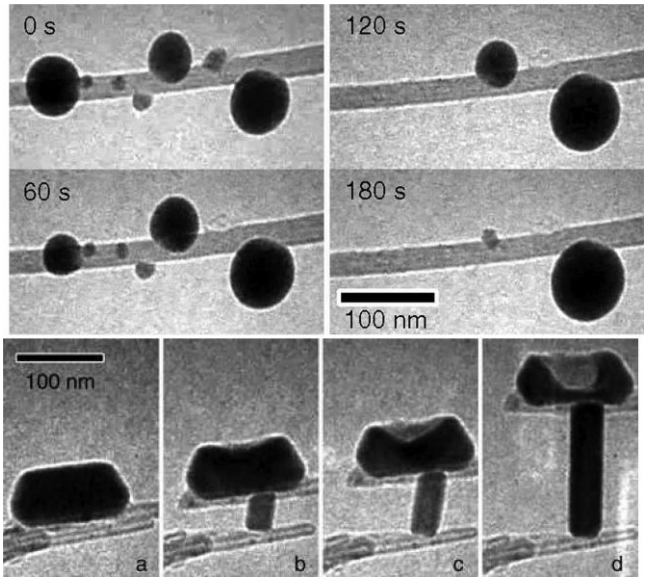


Figure 3. (top) TEM video images showing indium atom transport on a MWNT driven by electric field. Reproduced with permission from ref 71. Copyright 2004 Nature Publishing Group. (bottom) TEM video images (spanning 60 s) show a nanocrystal ram extension. Initially, two MWNTs lie in contact with one another, and a reservoir of indium atoms rests on the top nanotube. The driving current of 2.1 μA creates the ram, which pushes the MWNTs apart. Reproduced with permission from ref 74. Copyright 2005 American Chemical Society.

generated in (metallic) MWNT by two electrodes attached to a battery. It was found that the current can drag the indium atoms from one droplet adsorbed on the CNT surface (shrinking) to another such droplet (growing). When the dc current direction was reversed, the transport direction of indium atoms was also reversed.[72] Moreover, the In atoms were transported in the direction opposite to the direction of the electron flow. This observation was explained by using ab initio calculations,[73] which showed that isolated indium atoms adsorbed onto graphene and CNTs can transfer about one electron per atom to their surfaces. Therefore, the application of an electric field to the above system can cause the positively charged indium atoms, thermally diffusing around the droplets, to move in the direction opposite to the electron flow. This is due to the large direct force, F_d.

This material drag mechanism was implemented in the construction of a nanoscale manipulator,[74] as shown in Figure 3 (bottom). Here, two parallel MWNTs were initially in contact with each other, and a reservoir of indium atoms was placed on top of one of them. Once the electric current was passed between the CNTs, the transported In atoms started to grow into a ram, and pushed the two nanotubes apart. These results show that material manipulation along nanotubes could be successfully used in the building and control of nanostructures.[75]

In other studies, Fe[76] and Cu[77] nanoparticles were melted inside CNTs using high density electron currents and subsequently transported through them. Because the metal atoms were transported in the direction of the electron flow, they were probably dragged by the wind force, F_w. In Figure 4,

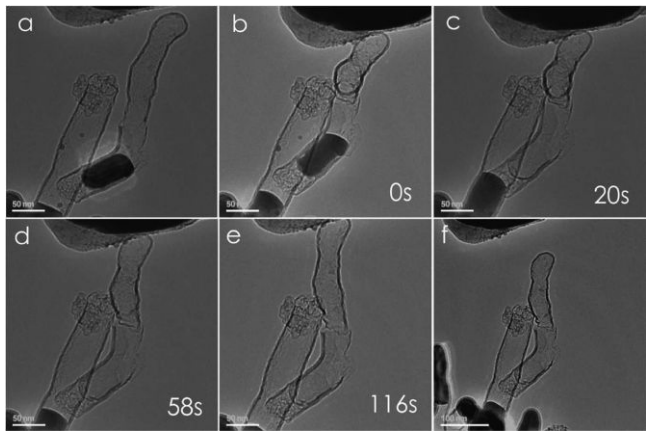


Figure 4. Time-resolved TEM images showing melted Sn flowing between two MWNTs in the presence of an electric current. Reproduced with permission from ref 78. Copyright 2009 American Chemical Society.

the transport of Sn atoms from one MWNT to another by the electric current is shown.[78] In another study, CuI was transported through MWNTs by pulsed electric currents,[79] which caused CuI decomposition and electromigration of the ions formed. Mercury was also dragged inside CNTs by electric fields.[80] Large molecules, such as LaC_{82} fullerenes and LaC_2 metal clusters, were set in motion inside the CNTs by electron irradiation.[81]

In recent years, graphene monolayers have also been prepared and intensively studied experimentally.[82–85] Atomic drag induced by electric currents was also used in cleaning graphene from contaminants[86,87] as well as manipulating matter along graphene.[88] As shown in Figure 5a, a thin layer of aluminum was first deposited on the graphene surface.[88] A charge transfer between the aluminum atoms and graphene allowed dragging of the atoms in applied electric fields. As shown in Figure 5b, aluminum atoms were first driven along graphene to the right in the direction of the horizontally applied electric field. When the electric field was reoriented to the vertical direction, the atoms changed their direction of

dx.doi.org/10.1021/cr200244h | Chem. Rev. 2013, 113, 3372–3390

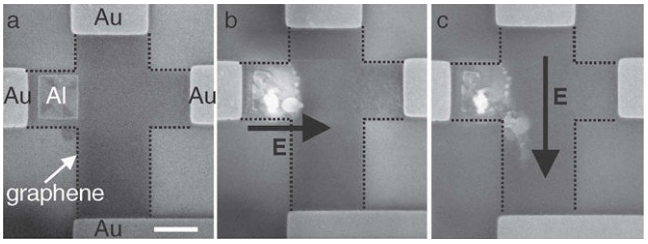


Figure 5. (a) SEM image of a graphene device with a crossroad configuration and aluminum deposited on the top. The scale bar represents 1 μm. (b,c) Motion of the aluminum after applying an electric field in different directions (indicated by the arrow). In (b) the voltage of V = 9 V was applied over t = 6 min and the current was I = 1.4 mA; in (c) V = 12.7 V, I = 1.63 mA, t = 9 min. Reproduced with permission from ref 88. Copyright 2011 Wiley-VCH.

motion to the bottom, as shown in Figure 5c. Here, the direct force was found to dominate over the wind force.

2.2. Electron Drag Induced by Flowing Polar Liquids

In analogy to the electron drag of atoms/molecules in CNTs, the "opposite effect" was also theoretically predicted.[89] Here, polar and ionic solutions flowing around metallic CNTs were able to drag its conduction electrons, as schematically shown in Figure 6. Initially, analogous to the electron drag in

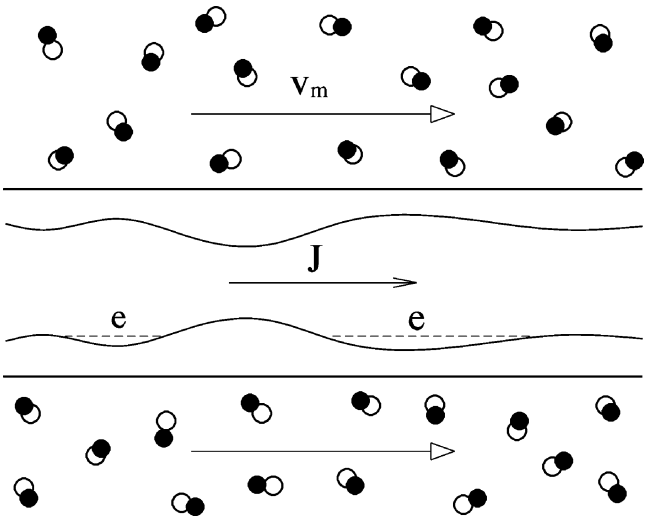


Figure 6. Scheme of a metallic CNT immersed in a polar liquid flowing along it with a velocity v_m. The molecules, denoted by pairs of circles for different atoms, coat the nanotube in the form of slipping layers, which drag the free carriers in the nanotube. Reproduced with permission from ref 52. Copyright 1999 American Physical Society.

materials,[55−57] two dragging mechanisms were proposed. In the first mechanism, it was suggested that an unidirectional phonon wind is generated in the CNT by the polar liquid flowing around it. Here, the phonons couple to the free CNT-electrons and drag them. In the second mechanism, it was speculated that the polar liquid (water) can partially localize the free CNT-electrons in fluctuating electrostatic potential wells and drag them when flowing.

In subsequent experiments, the molecular flow-induced electric currents were in fact observed.[90,91] Polar and ionic fluids, such as water, methanol, water−glycerol mixtures, and HCl solutions, flowing around a mesh of randomly ordered SWNTs between two contacts, successfully generated voltages and electric currents between the contacts.[90] As shown in Figure 7, the induced currents had a logarithmic dependence

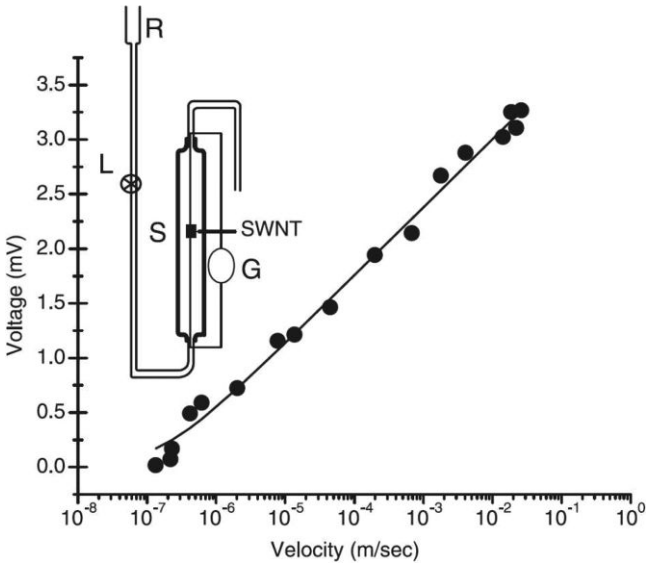


Figure 7. Variation of voltage V developed as a function of velocity u of water. Solid line is a fit to functional form as $V = \alpha \log(u\beta + 1)$, where α and β are constants. Inset shows the experimental setup, where R is the reservoir, L is the valve controlling the liquid flow, S is the cylindrical glass flow chamber, and G is the voltmeter. Reproduced with permission from ref 90. Copyright 2003 AAAS.

on the fluid flow rate. As expected,[52] the use of SWNTs was crucial for the generation of the current because they can provide the strongest electron localization and the closest contact between these electrons and the passing fluids. Similar experiments performed with MWNTs generated voltages about an order of magnitude smaller. On the other hand, liquid flow on graphite surfaces did not generate any measurable electrical signal.

The experimentally observed electric currents were explained by the presence of a fluctuating ratchet potential.[90] In this mechanism, ionic solutions flowing around the CNT can temporarily accumulate local charges close to the surface. These can generate Coulombic potential wells that localize the CNT electrons.[89] This potential has nonequilibrium fluctuations asymmetrically deformed by the flow velocity gradient near the CNT surface. This fluctuating asymmetric ratchet-like potential could drag the electrons[58] and produce the logarithmic dependence of the induced current on the flow velocity.

Later, the logarithmic dependence was explained slightly differently for CNT electron drag realized in ionic solutions.[92] It was proposed that the ions can adsorb onto CNT surfaces, where they can form, together with the first layer of water, a relatively rigid monolayer. Similar distributions are known to occur inside narrow CNTs and BNTs, as shown in Figure 21 (bottom). It was suggested that both the adsorbed ions and the solid-like water pinned to the CNT are dragged in a stick−slip motion by the flowing ionic solution. When a critical stress is reached, a local yield takes place, and the first layer of water together with the ions rapidly rearrange and slide on the CNT surfaces. The adsorbed ions move forward with their screening images in the CNTs,[93] and generate electron flows, analogous to the proposed electron drag mechanism.[89]

dx.doi.org/10.1021/cr200244h | Chem. Rev. 2013, 113, 3372−3390

In this model,[92] it was shown that the drift velocity of the CNT-adsorbed ions has a logarithmic dependence, $v_a = v_a^c \ln(v_0/v_c)$, on the flow velocity v_0, where v_a^c and v_c are constants. From this relationship, the induced currents and voltages were obtained as follows. If the electrons in the CNT have the drift velocity v_e, the electric current is $I = 2\pi r n_e e v_e$. The drift velocity, v_e, can be obtained from the approximate equation of motion for electrons inside the CNT:

$$m_e \frac{dv_e}{dt} = -m_e \frac{v_e}{\tau} - m_a \eta (v_e - v_a)\frac{n_a}{n_e} + eE \tag{4}$$

where τ is the relaxation time, η is the electronic friction coefficient, n_a is the concentration of the adsorbed ions, n_e is the concentration of electrons in the CNT, and E is the electric field inside the CNT.[92]

Two limiting solutions of eq 4 were considered. In the short circuit case, $E = 0$ in steady state ($dv_e/dt = 0$), and one can obtain that

$$v_e = \frac{(m_a/m_e)(n_a/n_e)\eta\tau v_a}{1 + (m_a/m_e)(n_a/n_e)\eta\tau}$$

$$I = \frac{\kappa}{1+\kappa} 2\pi r n_e e v_a \propto \ln v_0 \tag{5}$$

Here, the logarithmic dependence of v_a on v_0 was used. In the open circuit case, $v_e = 0$, so the voltage on the CNT is $U = LE$, where L is the CNT length. Therefore, eq 4 gives

$$U = \frac{L m_a \eta}{e}\frac{n_a}{n_e} v_a \propto \ln v_0 \tag{6}$$

This simple model gives the logarithmic dependence of the current/voltage on the flow velocity in both the short and the open circuit cases, as observed in experiments.[90]

Despite this success, it should be noted that the present assumption of ions being adsorbed onto the CNT within an ice-like water monolayer was deduced from studies of hydrated ions on MICA surfaces. Our recent quantum molecular dynamics simulations performed using TeraChem around 3 nm long metallic (4,4) CNTs did not reveal hydrated ion adsorption or ice at the nanotube surface (Na^+ was diffusing ~3−4 Å and Cl^- was ~4−5 Å above the CNT surface).

A combination of the above electron-material drag mechanisms was also experimentally tested.[94,95] In Figure 8, a scheme of the experimental setup is shown. When the current/voltage was applied between electrodes 3 and 4 ("motor" part, electrode 3 was grounded), water was dragged inside the metallic SWNT from region 3−4 to region 1−2. Two voltmeters, connected to electrodes 1 and 2 ("generator" part), detected the voltage difference between 1 and 2, generated by the water flow. It was suggested that Coulombic coupling between water dipoles and free electrons in the SWNT caused the drag mechanism. This is analogous to the initially proposed mechanism.[89]

2.3. Electron Drag Induced by Flowing Gases

Electron resistivity in solid-state materials is mainly caused by the scattering of electrons by other electrons, phonons, and impurities.[96] Analogously, the scattering of CNT-electrons from atoms and molecules in media surrounding the CNTs, such as gases[97] and ions in solutions,[98] can change their electronic transport properties. For example, it was found experimentally that the flow of N_2, Ar, and O_2 gases along the surfaces of CNTs generates electric current in them,[99] as shown in Figure 9. The observed induced potential difference was attributed to thermoelectric effects, which were caused by temperature gradients induced by the gas flow.

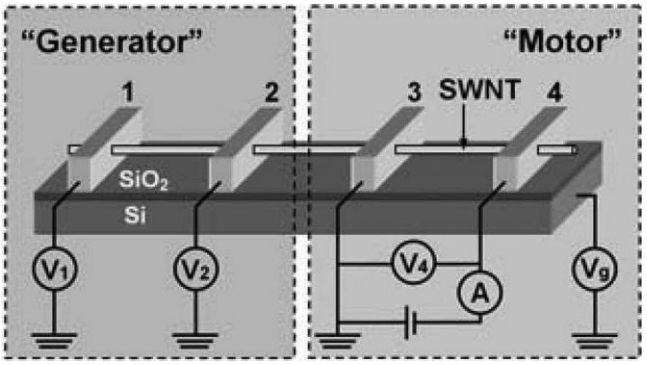


Figure 8. A suspended SWNT connected to four electrodes. Current/voltage is applied between electrodes 3 and 4 ("motor" part), and the induced electromotive force resulted in a voltage difference being measured between electrodes 1 and 2 ("generator" part) when the device is exposed to water vapor. Reproduced with permission from ref 94. Copyright 2008 Wiley-VCH.

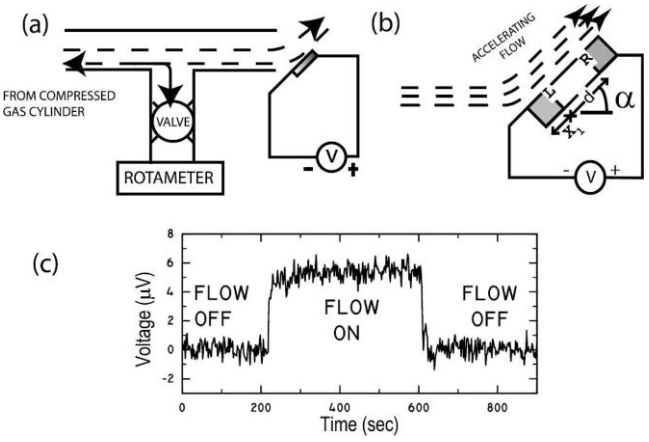


Figure 9. (a) Schematic of the general setup. The flow rate at the exit point is deduced from the measured flow rate at the side port using the rotameter. (b) Sample: Shaded portions marked the electrodes. The positive terminal of the voltmeter is connected to the right (R) of the sample of active length d kept at an angle $\alpha = \pi/4$ with respect to the horizontal axis. (c) Typical response of n-doped Ge for a flow of argon gas at 7 m/s. Reproduced with permission from ref 99. Copyright 2004 American Physical Society.

These thermoelectric phenomena can be explained as follows.[99] For the adiabatic steady-state inviscid flow of gas, Bernoulli's equation gives the pressure along a streamline:[100]

$$\frac{P}{P_0} = \left[1 - \frac{1}{2}(\gamma - 1)M^2\right]^{\gamma/\gamma-1} \approx 1 - \frac{\gamma}{2}M^2 \tag{7}$$

Here, $M = u/c$ is the Mach number, where u is the gas flow velocity and c is the velocity of sound, $\gamma = C_p/C_v$, where C_p (C_v) is the specific heat at constant pressure (volume), and P_0 is the maximum pressure at the point on the streamline (flow velocity is zero). The relative pressure difference between the left (L) side and right (R) side of the material sample is given by

$$\frac{P_L - P_R}{P_0} \approx \frac{\gamma}{2}(M_R^2 - M_L^2) \tag{8}$$

dx.doi.org/10.1021/cr200244h | Chem. Rev. 2013, 113, 3372−3390

From the ideal gas law, the fractional temperature difference is related to the pressure and density differences by $\Delta T/T = \Delta P/P - \Delta\rho/\rho$. If $M < 1$, $\Delta\rho$ is negligible, so $\Delta T/T \approx \Delta P/P$, and

$$\frac{\Delta T}{T_0} \approx \frac{\gamma}{2}(M_R^2 - M_L^2) \tag{9}$$

where $T_0 = (T_L + T_R)/2$ and $\Delta T = T_L - T_R > 0$. This temperature difference, ΔT, generates a voltage difference of

$$\Delta V = V_L - V_R = \frac{k}{2} T_0 S\gamma (M_R^2 - M_L^2) \tag{10}$$

where the Seebeck coefficient of the solid material, S, is positive for p-type and negative for n-type semiconductors. The factor k depends on the gas–solid interactions. In other regimes, this model also predicts that $\Delta V \propto M^2$. This is in good agreement with the experimental results.[99]

3. MATERIAL DRAG IN NANOTUBES INDUCED BY FLUIDIC FLOW

In recent years, nanofluidics in CNTs and other carbon-rich nanomaterials has been broadly explored. Initially, it was found, by classical molecular dynamics (MD) simulations,[101] that water, in adition to other atoms and molecules, can enter CNTs, due to the relatively large mutual van der Waals (vdW) coupling. In the following experiments, a fast passage of gases[102,103] and liquids[104−107] through CNT membranes was demonstrated. The atomic smoothness and hydrophobicity of CNTs lead to unusually low molecular friction and transport rates that were orders of magnitude higher than those expected according to classical fluid transport theories.[108] The passage rates of water and ionic solutions through CNTs and along their surfaces depend on their mutual interactions[109] and orientation.[110] Molecular transport inside BNTs was also examined.[111,112] The flow rates can be influenced by chemical functionalization[113] and electrostatic gating.[114] Recently, it has been also proposed that porous graphene forms selective sieves for ions[115] and other molecules in both the gas and the liquid phases.[116−118] The initial experiments were performed with DNA and other molecules passing through the pores.[119−122]

3.1. Coulombic Drag of Molecules Induced by Distant Flow

In the previous section, we discussed atomic and molecular drag in CNTs caused by electron–molecule scattering.[52,71,76,89,90,92] In recent years, using MD simulations, it has also been shown that molecules might be dragged on CNT surfaces when they Coulombically scatter at nanometer distances with molecules in polar[123] and ionic solutions[124] flowing through the nanotube interior. Analogously, charged particles moving outside the CNTs could drag charged peptides solvated in the nanotubes.[125] These "across-the-wall" molecular drag phenomena can broaden the range of options for controlling material transport on a nanoscale.

3.1.1. Dragging of Molecules on Nanotubes by Water Flowing through Their Interior. In the first successful demonstration of such across-the-wall molecular drag phenomena,[123] using classical MD simulations, it was shown that ions and highly polar molecules, such as the NH_3^+–$(CH{=}CH)_4$–CH_2–$(CH{=}CH)_6$–CO_2^- zwitterion, can be physisorbed on SWNTs and subsequently dragged by Coulombic scattering with the water passing through them under pressure.[104] The zwitterion dragging onto CNT by water is shown in Figure 10.

The approximate molecular parameters were obtained from ab initio quantum chemistry calculations using Gaussian 03,[126]

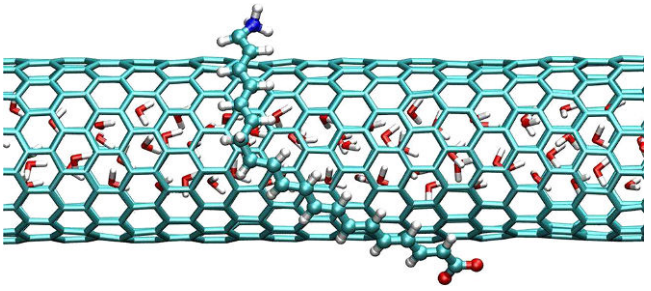


Figure 10. The NH_3^+–$(CH{=}CH)_4$–CH_2–$(CH{=}CH)_6$–CO_2^- zwitterion molecule adsorbed on the surface of the (14,0) SWNT driven by the flow of water molecules inside the CNT at $T = 300$ K. In the confined CNT geometry, the water molecules are transiently oriented in one or the other direction. However, they randomly switch between the orientations in longer simulations. The molecular orientation also switches, and its motion on the CNT surface looks like a free diffusion. Reproduced with permission from ref 123. Copyright 2006 American Chemical Society.

and were added to the CHARMM27 force field.[127] The system was placed in a (periodic) box with the dimensions 4.8 × 4.8 × 9.94 nm and simulated in the NVT ensemble (constant number of molecules, volume, and temperature) with NAMD.[128,129] The long-range electrostatic forces were computed by the particle-mesh Ewald method.[130] Langevin dynamics[131] was used at $T = 300$ K with a small damping coefficient of 0.01 ps^{-1} and the time step of 1 fs, to preserve the momentum of the dragged molecules (minimize its nonphysical dissipation by the reservoirs).[132] The tube was left free to vibrate, except for a few fixed atoms, and the water flow was induced by applying an unidirectional force on the oxygen atoms. The generated pressure of $P \approx 70$ atm[133] caused water molecules to flow with an average velocity of $\langle v_{wat} \rangle \approx 10-20$ m/s.

The Coulombic potential energy of the molecule adsorbed on the nanotube and coupled to all of the water molecules flowing inside the tube is

$$E_C \approx \sum_i q_i \varphi(r_i),\ \varphi(r) = \frac{1}{4\pi\varepsilon} \sum_j \frac{Q_j}{|r - r_j|} \tag{11}$$

Here, q_i and Q_j are the charges of the ith atom in the adsorbed molecule and jth atom in the water chain (O or H), respectively, with the coordinates r_i and r_j. The charges are effectively reduced by the size of the dielectric constant ε of the (semiconducting) nanotube.

In Figure 11, the molecular drag rate is illustrated on the ratio $R = v_m/v_w$ of the average velocities (total distances traversed) of the molecules or molecular ions on the CNT surface and water flowing inside the tube. The ratios R were obtained for different effective total charges q of the tested ions (model dielectric constant ε) in $t \approx 100$ ns trajectories. Because $R \approx 0.7-0.8$, the molecular drag is very efficient.

In this system, the zwitterion is attached (physisorbed) by vdW coupling to the (nonpolarizable) CNT and by Coulombic coupling to the water in its interior. It diffuses fast on the CNT surface, and its random motion is also influenced by the fluctuating and "shifting" electrostatic potential, $\varphi(r)$, generated by the flowing polar liquid.[134] The center of mass of the molecular diffusion trajectory shifts (about 100 times slower than its diffusion speed on the surface) with the fluctuating relief of $\varphi(r)$. The more polar is the molecule, the more deterministic is its motion, eventually resembling motion on an

dx.doi.org/10.1021/cr200244h | Chem. Rev. 2013, 113, 3372−3390

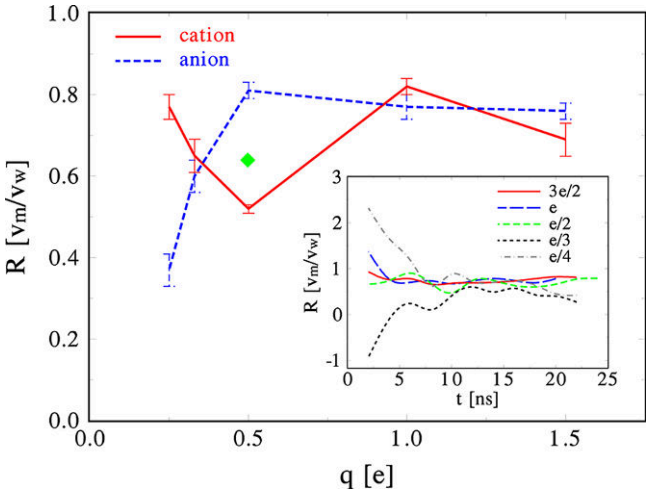


Figure 11. The ratio R of the average velocities (distances) of the adsorbed $CH_2{=}CH{-}CH{=}CH{-}NH_3^+$ and $CH_2{=}CH{-}CH{=}CH{-}CH_3{-}O^-$ ions (v_m), with different effective total charges q, and water (v_w) inside the (14,0) SWNT. The diamond at $q \approx 0.5$ applies to the $NH_3^+{-}(CH{=}CH)_4{-}CH_2{-}(CH{=}CH)_6{-}CO_2^-$ zwitterion molecule with correct (unscaled) charges. (inset) The ratio between the average speed of the $CH_2{=}CH{-}CH{=}CH{-}CH_3{-}O^-$ anion and the flowing water plotted with the time of driving (averaging). Reproduced with permission from ref 123. Copyright 2006 American Chemical Society.

"elastic transportation belt". Screening of the electric fields by the CNTs has not been considered here, but its possible effect can be very important (discussed later).

3.1.2. Dragging of Nanodroplets on Nanotubes by Ions Passing through Their Interior. The idea of across-the-wall Coulombic coupling was also theoretically tested in the dragging of nanodroplets of polar molecules adsorbed on CNTs and BNTs.[124] Figure 12 presents a nanodroplet with N_w = 400 water molecules adsorbed on the surface of a (10,0) SWNT at T = 300 K. The droplet is dragged by a distant single Na^+ (Cl^-) ion intercalated in the SWNT, when an electric field of ε_0 = 0.1 V/nm is applied along the tube. If the field is not very strong, the ion tends to diffuse in the nanotube region covered by the droplet, while slowly pulling the droplet forward. At larger fields, the ion can leave the droplet area, as discussed below.

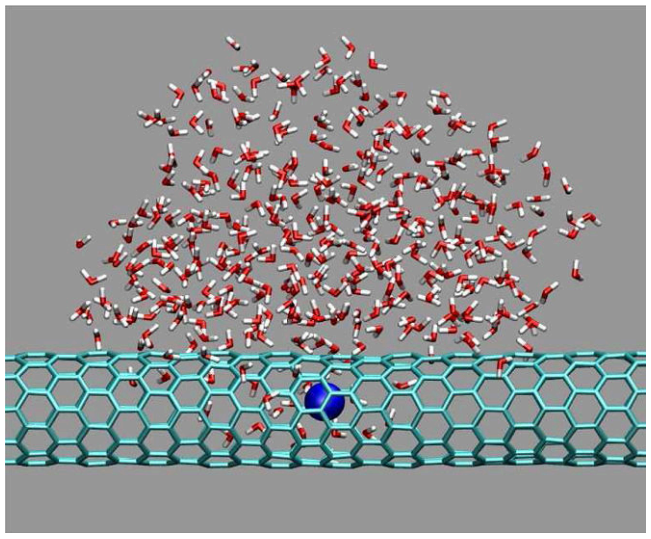


Figure 12. A nanodroplet of N_w = 400 water molecules dragged on the surface of (10,0) carbon nanotube by a single Na^+ ion intercalated inside the tube and driven by the electric field of ε_0 = 0.1 V/nm, applied along the tube z axis. Reproduced with permission from ref 124. Copyright 2008 American Physical Society.

If the system in Figure 12 is left to relax in the absence of an external electric field, a dynamical equilibrium is established (in the vapor and liquid phases). Here, a water nanodroplet condenses on the (nonpolarizable) CNTs around the ion, as on the other nanofibers.[135] The ion induces and is held in a dynamical polarization potential well formed in the droplet.

Figure 13 illustrates the Na^+ and Cl^- ion-droplet binding energies, E_b, obtained in the absence of external electric fields.

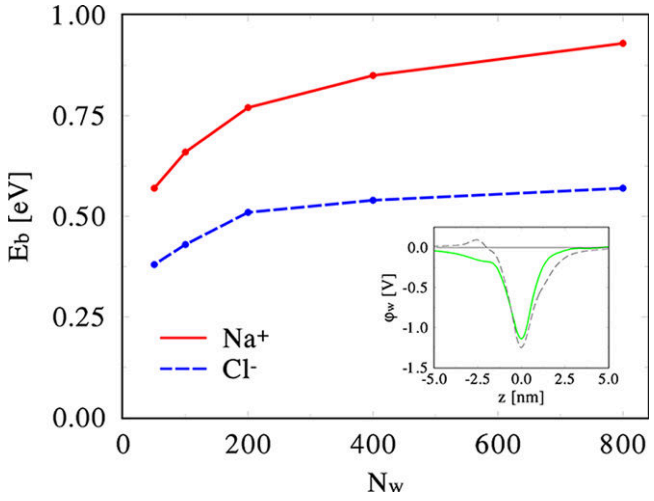


Figure 13. Binding energies, E_b, between Na^+ (Cl^-) ion, intercalated in a (10,0) CNT, and water nanodroplets of about N_w molecules, adsorbed on its surface (gas-phase molecules are neglected). (inset) Snapshots of the electrostatic potential φ_w along the axis of the nanotube with the intercalated Na^+ ion. The polarized water molecules create a steep potential well of a depth ~1 eV around the ion that moves together with it. Reproduced with permission from ref 124. Copyright 2008 American Physical Society.

The binding energies are several times smaller than the Na^+ and Cl^- bulk hydration energies of E_{solv} = 7.92 and 6.91 eV,[136] respectively. The binding energies saturate for larger droplets with N_w = 100 − 800 waters. The E_b energy can be estimated analytically by assuming that the ion is located at a distance $d \approx$ 0.35 nm above a flat surface of water with a dielectric constant of $\varepsilon_w \approx 80$. This gives the equation

$$E_b \approx -\frac{e^2}{4d}\left(\frac{\varepsilon_w - 1}{\varepsilon_w + 1}\right) \approx -1 \text{ eV} \qquad (12)$$

which is in good agreement with Figure 13.

Figure 14 shows the average velocities, v_w, of the nanodroplets with N_w water molecules in the system shown in Figure 12, when the electric field of ε_0 = 0.1 V/nm is applied along the (nonpolarizable) CNT. The velocities obtained are (1) proportional to the electric field, (2) they have practically the same values when Na^+ or Cl^- ions are used for the dragging, and (3) they largely decrease with the droplet size. Dragging the water nanodroplets by individual ions was also modeled on BNTs with highly polar surfaces.[40,112,137] The observed ring-like droplets were dragged about 40 times slower than on the CNTs.[124]

dx.doi.org/10.1021/cr200244h | Chem. Rev. 2013, 113, 3372−3390

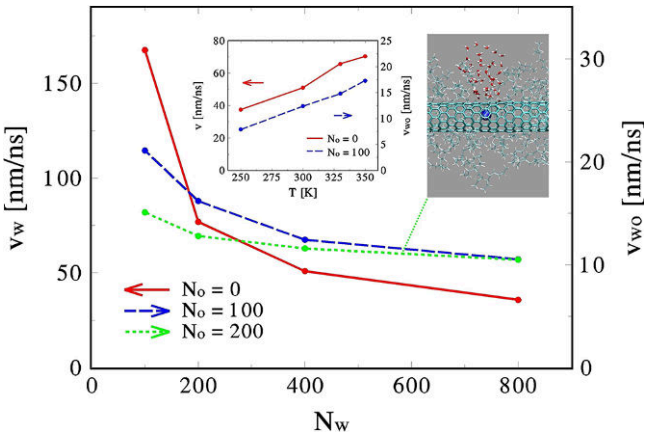


Figure 14. Dependence of the nanodroplet velocity, v_w, on the number of its water molecules N_w. The nanodroplet velocity, v_{wo}, in the presence of N_o = 100 and 200 octane molecules is also shown. (right inset) Visualization of the nanodroplet with N_w = 50 in N_o = 200 octane molecules. (left inset) Temperature dependence of the nanodroplet velocity for N_w = 400 and N_o = 0 and 100 octane molecules. Reproduced with permission from ref 124. Copyright 2008 American Physical Society.

Now, we briefly describe the nanodroplet drag motion on the nanotubes. Upon closer examination, we can find out that the water molecules and the ion move in a highly self-organized way, which closely resembles the motion of biological cells. The nanodroplet translation seems to be closer in character to sliding[138] than rolling,[139] due to partial wetting of the nanotube surfaces. The velocity of the macroscopic droplets moving both by sliding and by rolling motions is controlled by the momentum/energy dissipation of the water moving inside the droplet.[138] Both mechanisms qualitatively give the same dependence of the droplet velocity:

$$v_w \propto e\varepsilon/(r\eta) \tag{13}$$

Here, the droplet radius is $r \propto N_w^{1/3}$, and the water viscosity is $\eta \propto 1/T$.[140] The data shown in Figure 14 roughly confirm this dependence even for the motion of nanodroplets. Yet the driving velocity scales more steeply with the number of water molecules:

$$v_w \propto 1/N_w^{2/3} \tag{14}$$

The inset in Figure 14 shows that for N_w = 400 the temperature dependence of the droplet velocity is almost linear, $v_w \propto T$, as expected from eq 13. When the ion is placed inside the droplet, rather than inside the CNT, the velocity of the nanodroplet is about 20% larger.

An interesting situation occurs when the ions are driven in nanotubes fully submerged in water.[124] When (10,0) CNT was submerged in water and placed in the field of ε = 0.1 V/nm, the MD simulations gave the ion speeds of v_{Na^+} = 464.7, 622.5, and 733.7 m/s and v_{Cl^-} = 284.5, 401.6, and 547.9 m/s, at T = 240, 270, and 300 K, respectively. These speeds are limited only by a translationally invariant ion−water across-the-wall scattering.[134] Therefore, the speeds are 4−5 times larger than those of the ions dragging water nanodroplets in the same electric fields.

The role of screening in the across-the-wall molecular dragging was clarified by ab initio quantum mechanical calculations.[124] It was found that thin SWNTs,[34,141] such as (4,3) CNT, and all BNTs[30] have large band gaps, relatively small dielectric constants,[142] and they reduce the external electric fields in their interior by 10−25%. Interestingly, it was found that screening in metallic SWNTs does not block across-the-wall molecular dragging by individual ions or ionic solutions. Two ions separated by the wall of a metallic SWNT can still "see each other" via their screening charges that interact in the monolayer.[124] It turns out that the ion coupling is reduced by ∼70%. These results illustrate that across-the-wall Coulombic drag is possible even in metallic CNTs.

Drag in the Presence of Oil. The nanodroplet drag on CNTs is very different when oil is adsorbed onto their surfaces.[124] In Figure 14, the data presented show that N_o = 100 and 200 octane molecules adsorbed onto the CNT of the length of 5 nm can decrease the droplet velocity v_{wo} by an order of magnitude, due to friction between the water and the oil. Smaller droplets, N_w < 100, are attached to the ion by a narrow "neck" passing through the oil layer (right inset). Larger droplets are more spherical, are significantly submerged inside the oil, and in addition they share a very small surface area with the CNT. In analogy to water droplets present in bulk oil, their motion can be described by the Stokes law that seems to largely preserve its validity even on a nanoscale.[143,144] Here, it gives $F = -6\pi r\eta v_{wo}$, where $F = e\varepsilon_0$ = 16 pN is the drag force acting on the droplet, r is the droplet radius, and $\eta \approx$ 0.54 mPa s is the viscosity of octane at T = 300 K. For N_w = 100, one finds that $r \approx$ 3.5 Å, so v_{wo} = 4.5 m/s.

The effect of an "oily interface" can be also seen in our simulations presented in Figure 15. Here, it is clearly shown

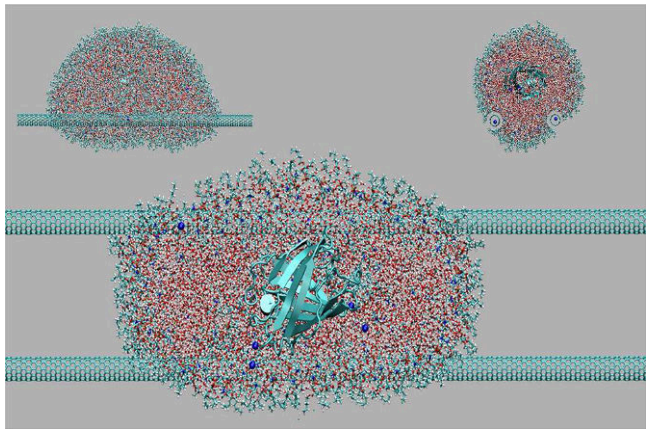


Figure 15. A reverse micelle formed by $N_w \approx$ 10 000 water molecules and 472 PPOPC phospholipids, which contains a GFP protein and 4 Na^+ ions neutralizing it (water is partly removed to see the protein, bottom and right top). It is driven by two Na^+ ions intercalated inside two CNTs.

that a reverse micelle[145] can be dragged on two (10,0) CNTs with one Na^+ ion present in each of the CNTs. The micelle is covered by a lipid monolayer, and it contains (hence can deliver) one GFP protein[146,147] with 4 Na^+ neutralizing ions.[148] The amphiphilic lipid molecules, 1,2-dipentanoyl-3-phosphatidylcholine (PPOPC), have hydrophobic chains with half the size of POPC, a common biological membrane phospholipid.[149] They allow the reverse micelle to keep a close distance between water and the CNT dragging ions, but they also prevent unfolding of the protein on the CNTs.[124] When the CNT-ions are driven by the electric field of ε_0 = 0.03 V/nm, the (neutral) reverse micelle is dragged with a speed of v < 0.2 nm/ns. If only a water droplet with N_w = 10 000 is dragged as shown in Figure 15 by an electric field of ε_0 = 0.1 V/nm, the

dx.doi.org/10.1021/cr200244h | *Chem. Rev.* 2013, 113, 3372−3390

droplet moves together with the ion pair at a speed of $v_w \approx 6.6$ nm/ns.

Ion Capture by Nanodroplets. When the ion−droplet complex is driven by large electric fields and/or when the droplet is very small, the ion can relatively easily escape and later be recaught by the nanodroplet (in the presence of periodic boundary conditions).

In Figure 16, we present the MD simulation trajectory of a Na^+ ion inside a (10,0) CNT coupled to a nanodroplet with N_w

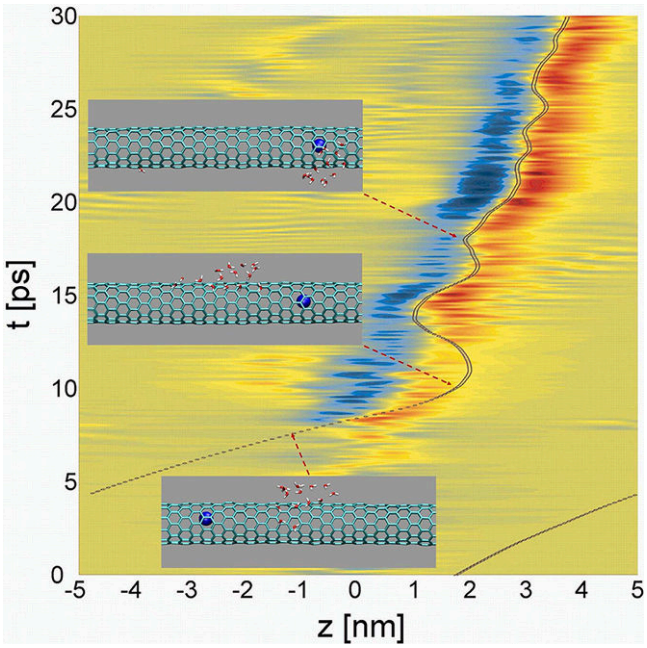


Figure 16. The trajectory of a Na^+ ion inside a (10,0) CNT, which is coupled to a water nanodroplet with $N_w = 20$ in the field of $\mathcal{E} = 0.02$ V/nm. During the simulations, the ion is released and recaught by the nanodroplet. The axial position and the time of the ion motion are shown on the horizontal and vertical axes, respectively. The electric field generated by the water molecules along the CNT axis is plotted by contours. Reproduced with permission from ref 124. Copyright 2008 American Physical Society.

= 20 water molecules in the field of $\varepsilon = 0.02$ V/nm.[124] The ion trajectory is shown by the dark line, and the induced electric field along the CNT axis created by the ion-polarized droplet is plotted by contours. The neighboring regions with positive/negative fields (different colors) correspond to the sides of the potential well that forms around the ion.

In the electric field used, the ion manages to leave this small nanodroplet, goes once around the tube, and reapproaches the droplet with a velocity of $v_{ini} \approx 1400$ m/s (bottom) at $t < 7$ ps. When the ion gets closer to the droplet, its water molecules become highly polarized (inset at $z = -1.3$ nm, $t = 7$ ps). The ion first passes around the droplet, just to be attracted back by several chained molecules protruding from the droplet ($z = 1.7$ nm, $t = 10$ ps). During the deceleration of the fast moving ion, its kinetic energy is converted into a Coulombic potential energy of the chained water molecules. This energy is released in the form of heating of the nanodroplet during the following short oscillations of the ion in the droplet, followed by its recapture ($z = 2$ nm, $t = 18$ ps). Eventually, the ion−droplet pair cools on the nanotube and moves at a much smaller velocity of $v_{end} \approx 130$ m/s. The observed transient oscillations during the ion−droplet pair formation resemble oscillations accompanying the formation of quasiparticles.[150]

3.1.3. Dragging of Solvated DNA on Nanotubes by Ionic Solutions Flowing through Their Interior. Across-the-wall Coulombic coupling might also be used to drag molecules adsorbed on CNTs solvated in ionic solutions and deliver drugs.[151−154] In Figure 17 (top), we show our MD

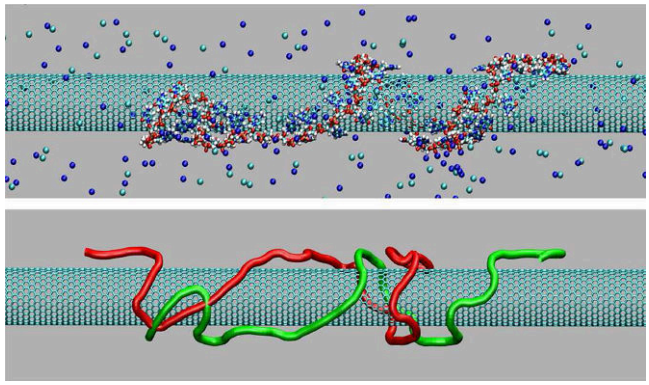


Figure 17. (top) A 50-base long single strand DNA molecule, with the sequence CCTTCAGTGG CCGGTCATTG ATGAAGCCCT GAGGAACAAG GACACTCCGG,[156] driven on the surface of a (25,0) CNT (periodic unit cell of 65.5 × 65.5 × 293.8 Å) by the ionic solution flowing inside. (bottom) Motion of the DNA backbone to the left is clearly visible ($t = 0$, green strand; $t = 7.4$ ns, red strand).

simulations of a 50-base long single strand DNA molecule that binds by $\pi-\pi$ interactions[155] to the surface of the (25,0) (semiconducting) CNT. Outside the nanotube, 49 Na^+ cations are used to neutralize the DNA in 33 600 water molecules. In addition, 100 Na^+ and 100 Cl^- ions are added to model the physiological salt concentration (1%). The neutral ionic solution inside the nanotube (periodic boundary conditions) consists of 1850 water molecules, as well as 15 Na^+ and 15 Cl^- ions.

When the ionic solution inside the CNT was flowing to the left under the applied pressure of $P \approx 70$ atm at $T = 350$ K, the DNA was dragged with the average speed of $v \approx 0.3$ nm/ns, as seen in Figure 17 (bottom). The DNA molecules solvated in ionic solutions could also be dragged on CNT surfaces by electric currents passing through the CNTs.[89] In principle, the molecular drag might also operate on graphene when ionic solutions are pumped on its other side.[157]

3.1.4. Guided Self-Assembly of Filled Micelles on Nanotubes. Hydrated micelles formed by amphiphilic molecules and filled with drugs[158] and peptides[159] that are poorly soluble in water might be able to form highly efficient nanomedicines.[160] Recently, by using coarse-grained MD (CGMD) simulations, it was shown that such drug-filled micelles could be self-assembled in a controlled manner by a molecular drag on the surfaces of CNTs filled with drug molecules.[161] When the CNTs are placed in water with solvated lipids,[162,163] lipid hemimicelles[164] or cylindrical micelles[165] start to form onto their hydrophobic surfaces.[166−168] If the solution flows along the CNT and the drug molecules in its interior are pressurized from one side, the pro-micelles are dragged on the CNT surface, filled with drug molecules at the CNT tips, and sequentially released, in a process analogous to nanoscopic jets.[169] Drug molecules filling the micelles could be supported through the CNT interior, and the lipids might be continuously adsorbed on the CNT surface

dx.doi.org/10.1021/cr200244h | *Chem. Rev.* 2013, 113, 3372−3390

from the solution. In a related example of dip-pen nanolithography,[170] molecules are deposited on material surfaces by nanoscopic tips.

This idea was tested for lipid molecules that have one or two hydrophilic heads and a single hydrophobic tail, $[CH_3(CH_2)_{14}CH((CH_2OCH_2CH_2)_2(CH_2COCH_2))_2H]$.[161] The CNT-guided self-assembly of filled micelles was modeled using CGMD simulations[167,171−175] with the Martini 2.0 force field[176] implemented in the NAMD package.[128,129,177] Coarse graining of the lipids was performed through a four-to-one atom-mapping procedure,[171] where every four non-hydrogen atoms in the lipids are modeled as a single bead. The coarse-grained (CG) hydrophobic tails were represented by the C_1-type beads,[176] and the hydrophilic heads as the N_a-type and N_0-type beads, respectively. The coarse-grained double headed lipid is shown in the inset of Figure 18. The honeycomb

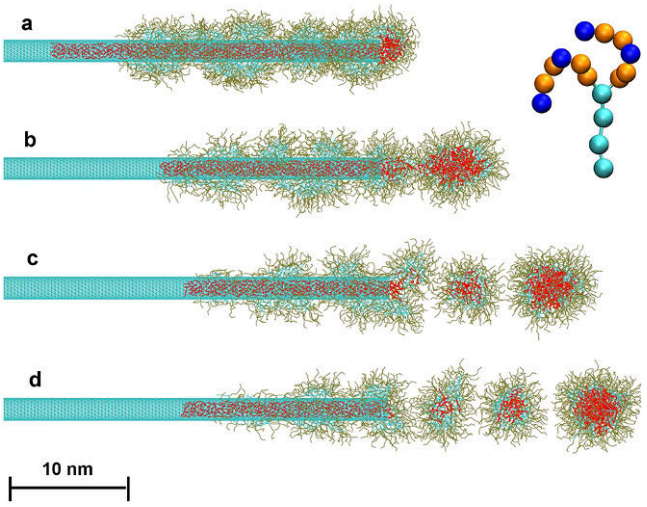


Figure 18. Controlled self-assembly of hydrated double-headed lipid micelles filled with hexadecane. (a) Lipids deposited on the CNT form random hemimicelles. Soon after application of the forces on the water and hexadecane molecules, the first hemimicelle covers the CNT tip. (b) The first micelle filled with hexadecane is formed at the CNT tip within ∼4 ns. (c,d) After another ∼10 ns, two more micelles are sequentially formed. The inset shows a single biheaded lipid molecule. Reproduced with permission from ref 161. Copyright 2011 American Chemical Society.

structure of CNT was reduced to a triangular lattice of CG beads,[175] where every three carbons in the graphene are modeled as a SC_4-type bead and the nonbonded interactions between the beads are defined in the Martini 2.0 force field.[176] Every four water molecules are united into a single P_4-type bead, and the hydrophobic hexadecane molecules, $CH_3(CH_2)_{14}CH_3$, filling the CNT were modeled by the C_1-type beads. The Langevin piston method has the damping coefficient of 1 ps^{-1} and time step of 15 fs. To prevent artificial freezing of the CGMD water at low damping, antifreeze water beads (8% of the total normal water beads) were used.

In the simulations, 450 lipids were placed on the surface of the (40,0) CG CNT, 400 hexadecane molecules were placed in its interior, and the system was equilibrated in CG water for t = 20 ns at T = 350 K. The equilibrated lipids wrap around the fixed CNT and form hemimicellar structures,[166,178,179] as shown in Figure 18a. When the force of f_1 = 2.08 pN oriented along the CNT toward its right tip was applied to each water bead, water flew with a velocity of $v \approx 1.5$ nm/ns and dragged the lipids onto the CNT. The molecules inside the CNT were pressurized in the same direction by a force of f_2 = 1.39 pN, applied on each of their beads. Using these forces, the velocities of the lipids and the hexadecane molecules were tuned so that they would be similar.

Upon application of these forces, the lipid and hexadecane molecules start to move toward the CNT tip, and soon the first hemimicelle covers the CNT tip, as seen in Figure 18a. Within 4 ns, the first micelle of diameter of $d \approx 5$ nm containing ∼100 hexadecane molecules is formed and detached from the CNT tip, as seen in Figure 18b. When it leaves, the remaining lipids and hexadecane molecules move forward, and the next hemimicelle covers the CNT tip in a similar fashion. The second filled micelle has a diameter of $d \approx 3$ nm, and it contains ∼40 molecules. The third micelle then is created within ∼10 ns after the first one, and so on. The kinetically stable micelles thus formed have different sizes, because the progression of both sets of molecules is not steady when their amounts are decreasing. Their sizes as well as the degree of filling can be controlled by the system parameters. It should be noted that in coarse-grained modeling, the system dynamics is about ∼4 times faster than in atomistic modeling (lack of structure in the CG systems).

3.2. Electrokinetic Drag of Molecules

The molecular drag phenomena discussed above are based on the mutual scattering of ions and molecules at relatively large distances (across the nanotube wall). The scattering of molecules at small distances, typically taking part in the same medium, can lead to various other drag phenomena. We will now describe some of these phenomena in CNTs and briefly discuss their possible modeling.

3.2.1. Modeling of Electrokinetic Phenomena. Electrokinetic phenomena in microchannels can be described by classical continuum theories,[180,181] using the Poisson−Boltzmann and Navier−Stokes equations.[182] These equations need to be solved simultaneously under proper boundary conditions in the nanochannels to obtain the fluid flow rates. The microscopic description breaks down in nanochannels,[183] but it can be partially corrected by including the finite sizes of ions,[184] nonelectrostatic interactions,[185] the dependence of the solution permittivity on the field strength,[186] the walls,[187] discrete solvent,[188] and other effects.[189−191] Even though some of the correction terms in the classical transport equations can be extracted from MD simulations,[182] a precise description of the electrokinetic transport in nanochannels can be obtained only from full MD or QM/MD simulations. Below, we present several typical examples of these simulations as performed in CNTs.

3.2.2. Electrophoretic Drag in Nanotubes. Charged colloidal particles have electric double layers (EDL) around them.[192] The EDL parameters are determined by the character of the particle and the solvent. In the presence of an electric field, the charged particle and its EDL can move to some extent separately, which in turn allows it to define and measure the so-called ζ-potential of the particle. This electric-field dragging of charged particles through solvents is called electrophoresis. For example, it was shown by MD simulations[193−195] and experiments that individual biological molecules, such as DNA, RNA, and proteins, could be dragged by electrophoresis through surfactant,[196] inorganic,[197] and silicon nanotubes.[180,198] The moving particles can also drag a lot of solvent

dx.doi.org/10.1021/cr200244h | Chem. Rev. 2013, 113, 3372−3390

molecules with them,[199] especially in the highly confined volumes present inside the nanotubes.

3.2.3. Electroosmotic Drag in Nanotubes. There is also a great practical interest in the passage of charged molecules and nanoparticles through membranes formed by CNTs[104] and other nanoscale materials.[200] In osmosis, typically one type of solvated molecules is unable to pass through the nanochannels in such a membrane, while the other components can pass through it.[201] When the blocked molecule is present at different concentrations on both sides of the channel, the other components can flow against its concentration gradient (solvation) and generate a pressure gradient (osmotic pressure) to stabilize the chemical potentials. CNTs have been used in osmosis, because small ions, with tightly bound hydration shells, are not able to enter narrow nanotubes.[202−204] For example, the critical diameter of nanopores for the entrance of individual hydrated Na^+ ions is $d \approx 7$ Å. This corresponds to both the (5,5) CNT[202,205] and the (5,5) BNT.[111,206,207] However, hydrated ions might still be able to enter such narrow CNTs at higher ion concentrations,[204] when the nanotubes are charged[208] or functionalized,[203,113] at high temperatures or in the presence of ultrasound.[209]

Figure 19 illustrates MD simulations of the osmotic flow through two hexagonally packed CNT-membranes, where each

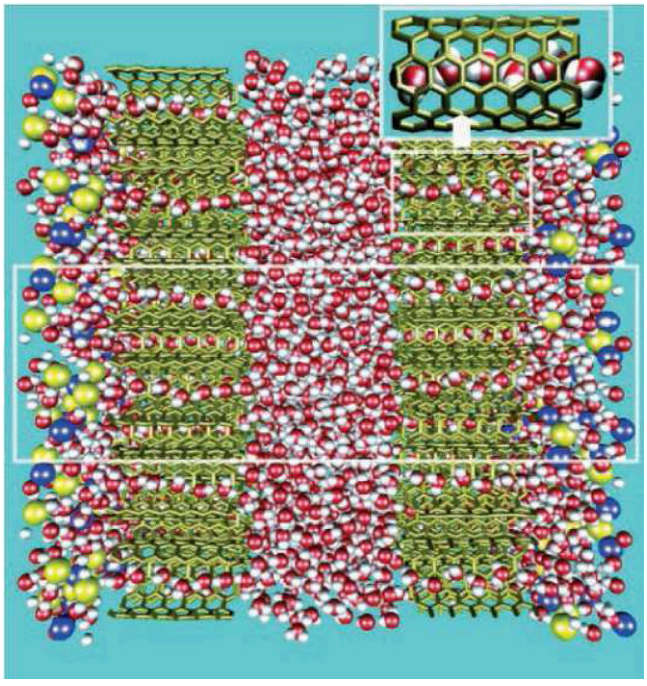


Figure 19. Snapshot of MD simulations of osmotic flow in CNTs. The pure water (middle) compartment is separated from the NaCl salt solution by two membranes of hexagonally packed CNTs. Only water can pass through the CNTs and flow in the compartment containing NaCl. Reproduced with permission from ref 210. Copyright 2003 National Academy of Sciences.

CNT is of (6,6) "armchair" type with length and diameter of 13.4 and 8.1 Å, respectively.[210] Two compartments are seen, one filled with pure water and the other with an aqueous solution of NaCl at an initial concentration of 5.8 M. The subnanometer pores of the CNTs permit the transport of water molecules between the two compartments, but not that of hydrated Na^+ and Cl^- ions. The resulting osmotic imbalance drives water to flow from the pure water compartment to the salt-solution compartment, thus gradually draining the pure water compartment.[210,211] A reverse osmosis can also be realized in this system.[212,213] By applying an external pressure on the reservoir with the ionic solution,[214] water can be transported with the ionic concentration gradient through the semipermeable CNTs into the reservoir with pure water.

In electroosmosis, external electric fields can induce the flow of ionic solutions through a channel.[192] Typically, the channel walls are partially charged due to the chemical groups attached to them. Therefore, opposite charged ions become Coulombically attracted to the charged walls and preferentially enter the nanochannel from the ionic solution. Once the electric field is applied along the channel, the ions that are prevalent in it are driven by the field, and as they move they drag the solution. Analogously, when an ionic solution flows through a CNT with charged walls in the presence of an electric field, the electroosmotic flow of water can occur.[114,208,215−217] Because of high localization, its flow direction might be opposite that predicted by continuum models.[218]

If the tips of a narrow CNT are modified with polar functional groups, ions of only one charge might be able to selectively enter the CNT from the solution, which can be then driven by electroosmosis in the presence of electric fields.[113,203] Figure 20 shows a model (16,16) SWNT functionalized with

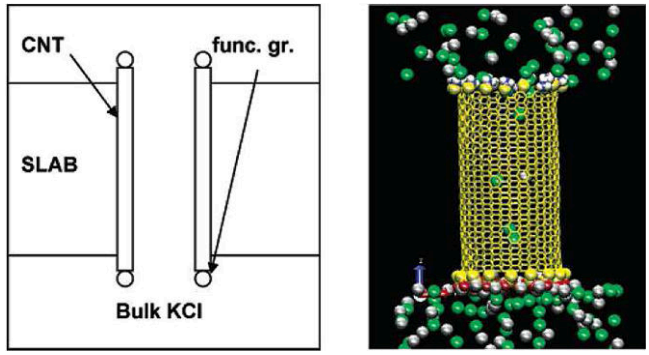


Figure 20. Schematic (left) and visualization of MD simulations (right) of a functionalized CNT inserted in a slab and solvated in a bath of 1.5 M KCl. One $CH_2-NH_3^+$ per carbon ring is attached to the top, and one CH_2-COO^- is attached at the bottom. Chloride ions are shown in darker shade. Water molecules are not shown. Chloride occupancy is higher than potassium. A buildup of potassium ions near the COO^- carboxylate ion is also observed. Reproduced with permission from ref 203. Copyright 2003 American Chemical Society.

$CH_2-NH_3^+$ groups attached at the top CNT end and CH_2-COO^- groups attached at the bottom CNT end.[203] The tube was placed in a membrane-mimic slab with properties similar to those of a lipid bilayer, and the system was solvated in 1.5 M KCl solution. When an electric field of $E = 0.15$ V/nm was used to drive the ions through the nanotube, the Cl^- ion flow through the CNTs was much higher than the K^+ flow. This was related to the fact that the K^+ ions were more tightly (electrostatically) bound to the COO^- groups at the nanotube entrance. This is in turn generated a large energy barrier and reduced their occupancy in the tube.

Related electrokinetic phenomena can occur in nanochannels even if both types of ions can enter into them, since the ions can be localized at different cross-section regions of the channels and/or move differently. For example, it was shown both experimentally and theoretically that EDL can exist at

nonpolar neutral nanochannel walls.[219−221] This is due to different distributions of hydrated ions at the water−wall interface. Even though neither (positive or negative) ions are attached to the walls, such as in typical electroosmotic phenomena, the fact alone that they are differently distributed at the walls can in fact lead to electroosmosis.

Recently, we studied these phenomena using classical MD simulations in narrow CNTs and BNTs filled with individual hydrated monovalent ions and their neutral solutions. In Figure 21 (top), we show the number of water molecules passing

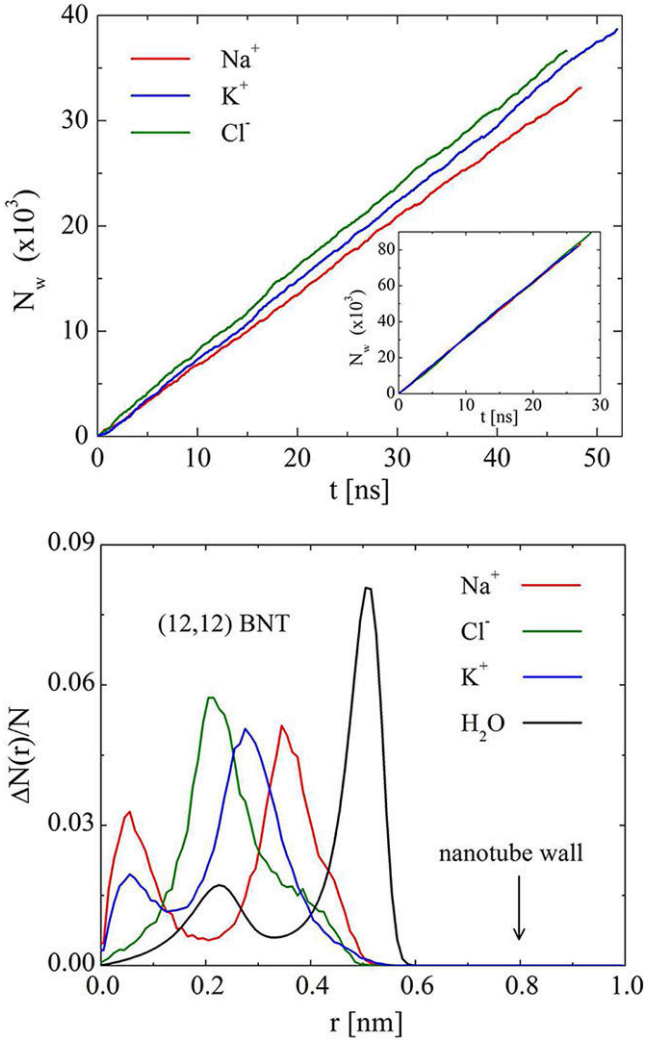


Figure 21. (top) The time dependence of the number of ions (N_w) passing through the (12,12) BNT in systems with a single hydrated Na^+, K^+, or Cl^- ion. (bottom) Normalized particle distribution profiles, $N(r)/N$, of Na^+, K^+, and Cl^- ions and water oxygens in the (12,12) BNT. The profiles are obtained by averaging over the whole simulation trajectories.

through the (12,12) BNT (length of $l \approx 10$ nm and partial charges of $q_B = q_N = e$[112]) when a single hydrated Na^+, K^+, or Cl^- ion is driven by the electric field of $\varepsilon = 0.11$ V/nm at $T = 300$ K, with electrostatic periodic boundary conditions applied.[130] We can clearly see that the drag rate of water is largest for Cl^-, it is smaller for K^+, and is smallest for Na^+. In the (12,12) CNT, the water drag rates for these ions are ∼4.5 times larger and practically identical to each other. The much larger flow rates in the CNT can be understood from the enhanced friction of flowing water in the polar BNT.

The individual drag rates can be understood from the radial distributions of ions in these systems, shown for the (12,12) BNT in Figure 21 (bottom); in the CNT, all of the distributions are shifted ∼1 Å away from the wall. We can clearly see that the distances of ions from the (12,12) BNT wall correlate with their water drag rates in this system. Therefore, these rates might originate in different "friction" of the ions with the walls. In (nonpolarizable) CNTs, the ion−wall friction is small, independent of the ion−wall distance, so the drag rates are practically the same for different ions. In BNTs, this ion−wall friction is larger, because the ion−wall distances are smaller than in CNTs and the BNT wall is effectively corrugated (polarity). Different ions then experience different frictions. When neutral solutions are driven in these systems, the water drag rate is also nonzero, but the phenomena that are present are more complex.

3.2.4. Other Fluidic Drag Mechanisms. The presence of EDL in channels can lead to other transport phenomena. For example, the generation of an electric current by pressure, called a streaming current, is a reverse effect to the elecroosmotic flow.[222] When an ionic solution flows under hydrostatic pressure through a channel with charged walls, counterions adjacent to the charged walls are carried downstream and generate an electric (streaming) current.

The streaming current was proposed to explain the voltages/currents generated by polar/charged liquids flowing around CNTs.[90] If the CNTs are charged after chemical treatment, the flow-induced voltages/currents generated in the CNTs might be caused by the streaming potential generated by the flowing "Debye layer" of counterions with positive charges on the nanotube surface.[223] Although it is likely that this mechanism can be observed in CNTs, this is probably not the main effect in the observed drag phenomena. This mechanism seems to contradict the fact that the flow-induced voltages that were observed were ∼10 times smaller in MWNTs than in SWNTs. It would also require large liquid flow rates and result in a linear dependence of the current on the flow rates.[224] In principle, new effects resulting from the combination of these phenomena might also exist in these systems.

Molecules in thin channels can also be dragged by capillary forces when the (vdW and Coulombic) liquid−surface coupling is stronger than the liquid−liquid coupling.[42,43,107,225−231] For example, DNA can spontaneously enter into CNTs,[232] due to capillary driving forces.[107] Recently, it has also been proposed that when external charges are asymmetrically positioned close to CNTs and their positions are fixed, water flow can pass without stopping through the nanotube connecting the two reservoirs.[233] The presence of such a flow would obviously break the laws of thermodynamics.[234] Later, it was shown that while static electric fields alone cannot pump fluids (equilibrium), periodically oscillated oscillations (nonequilibrium) can pump water in CNTs.[110,235−238] Other related scenarios might in principle lead to new drag phenomena, but one should carefully separate them from effects caused by potential numerical errors inherent in the simulations. It should always be kept in mind that drag requires the presence of both asymmetry and nonequilibrium.[58]

dx.doi.org/10.1021/cr200244h | Chem. Rev. 2013, 113, 3372−3390

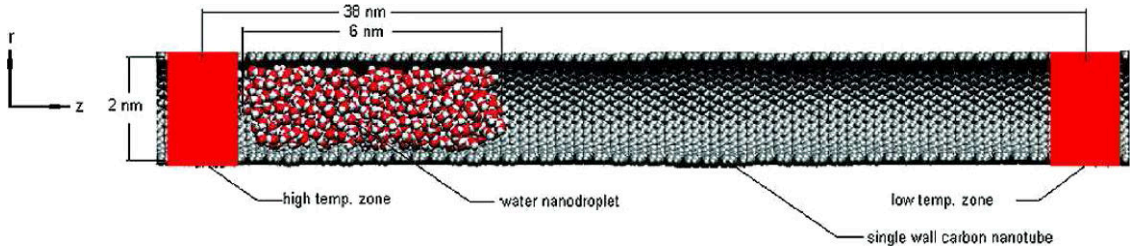


Figure 22. Schematic representation of the water nanodroplet confined inside a CNT. A thermal gradient is imposed by heating the end sections of the CNT. Reproduced with permission from ref 245. Copyright 2009 American Chemical Society.

4. MATERIAL DRAG IN NANOTUBES INDUCED BY MECHANISTIC MEANS

In analogy to electron drag induced by scattering with hot phonons in solids,[57] molecules can also be dragged by scattering with nonequilibrium phonons asymmetrically distributed in real and/or momentum spaces.[89] We will now discuss molecular drag inside CNTs and on their surfaces induced by their vibrations and rotations.

4.1. Thermal Gradient Drag of Molecular Assemblies

In thermophoresis, a heat flow produced in materials by thermal gradients can drag molecules. It was shown by MD simulations that thermophoresis can drag nanoparticles (NP)[239−241] and short CNTs[242] into the interior of large CNTs. If the temperature gradient is ∇T (roughly K per nm), the thermophoretic driving force in the linear regime is

$$F_{th} \propto k\nabla T \tag{15}$$

where k is a constant related to the coupling efficiency between the CNT phonons and the NP.[240,243] At small driving velocities acquired by the NPs, one can assume that the frictional force on the NP is given by

$$F_{fr} \approx A\mu v \tag{16}$$

Here, A is the NP−CNT contact area, μ is the frictional coefficient between them, and v is the velocity of the nanoparticle. In a steady state, the driving force is balanced by the frictional force, $F_{th} = F_{fr}$, which gives the average velocity of the NP proportional to the temperature gradient, $v \propto \nabla T$.

Thermophoresis can also drag fluids inside CNTs.[244−246] In the MD simulations shown in Figure 22, a zigzag (30,0) CNT is subjected to a thermal gradient of $\nabla T \approx 1$ K/nm, imposed along the CNT.[245] In this thermal gradient, a nanodroplet of $N_w = 514$ water molecules is dragged inside the CNT with a velocity of $v \approx 10-30$ nm/ns. These velocities are relatively large due to the ideal CNTs used in modeling, which lack surface defects that might slow the molecular motion. It is likely that nonlinearities play a relatively minor role in this dragging. Similar velocities were observed in MD simulations of the dragged gold NP,[240] the dragged zwitterion in Figure 10, and the water nanodroplet dragged in oil, as shown in Figure 14.

Recently, gold nanoflakes attached to suspended CNTs were experimentally dragged by using thermophoresis.[247] As in the SEM results shown in Figure 23, the cargo was easily movable by an AFM tip between different positions. When an electric current of $I = 0.06$ mA was applied along the CNT stretched between two electrodes, with a potential difference of $U = 3.3$ V, the gold flake first melted. This is because the electric current created a thermal gradient along the CNT, with a maximum temperature of $T \approx 1300$ K present in its center. The nanodroplet formed was dragged along the thermal gradient

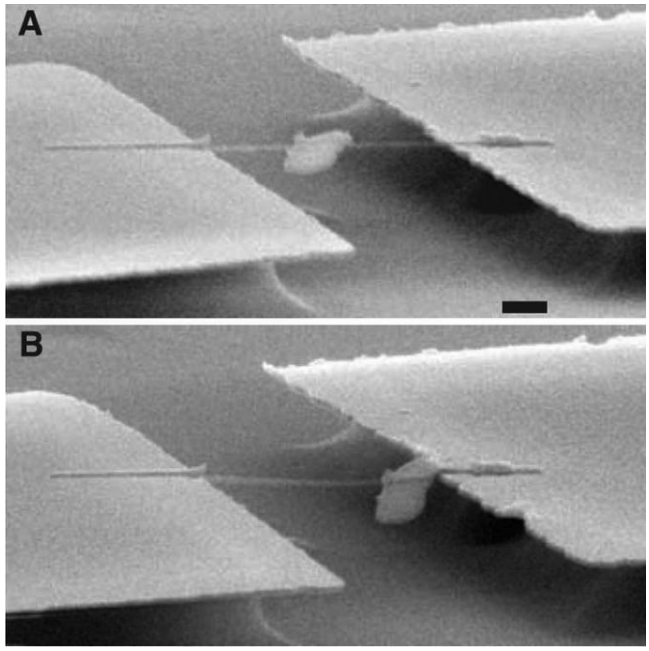


Figure 23. Scanning electron microscope (SEM) images of one device where the central object attached to the CNT in (A) has been moved via an AFM tip to its position in (B). Scale bar in (A): 300 nm. Reproduced with permission from ref 247. Copyright 2008 AAAS.

with a maximum velocity of $v \approx 500$ nm/s. Sometimes the droplet also rotated around the CNT. When the electric current orientation was inverted, the droplet moved in the same direction, proving a (predominantly) phonon origin of the drag caused by the temperature gradient. These results are in contrast with earlier studies of the current drag, where (cold) indium nanodroplets moved on CNTs ($v \approx 1-2$ nm/s) in the opposite direction upon current reversal.[71]

4.2. Coherent Phonon Drag of Nanodroplets

Coherent phonon waves (CNT vibrations), rather than a flux of thermal phonons, can also drag molecules into the interior and onto the surfaces of CNTs. For example, it was shown by MD simulations that helium atoms and water molecules could be pushed through deformed CNTs.[248−254] The unidirectionally propagating CNT deformations (waves) scatter with atoms and molecules intercalated in their interior or attached to them, pass momentum to them, and translate them along the CNT.

Recently, the drag of water nanodroplets on CNT surfaces by coherent transversal acoustic waves (TA phonons) was also observed using MD simulations.[255] The system is shown in Figure 24 (inset), where a nanodroplet with $N_w = 1000$ waters is adsorbed onto the (10,0) CNT. The tube is aligned along the z axis, groups of atoms at its two ends were fixed to block it

dx.doi.org/10.1021/cr200244h | Chem. Rev. 2013, 113, 3372−3390

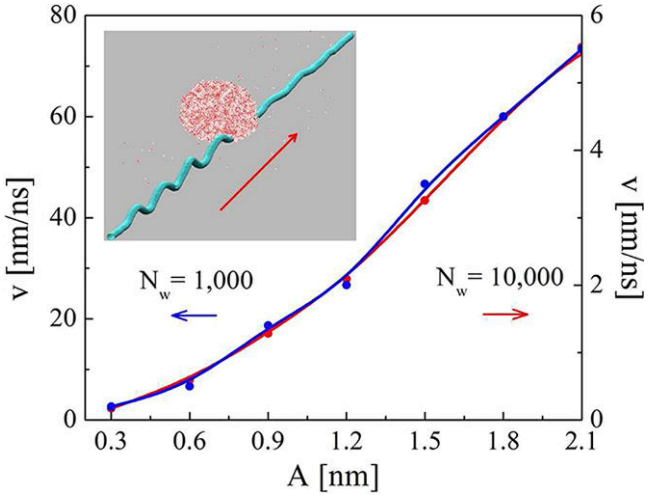


Figure 24. Dragging of nanodroplets with $N_w = 10^3$ (inset) and $N_w = 10^4$ waters on CNTs by coherent vibration waves. The droplet velocities are shown in dependence on the vibration amplitude A of the linearly polarized driving wave with the frequency of $\omega = 208$ GHz. Reproduced with permission from ref 255. Copyright 2012 American Chemical Society.

from shifting, and the tube was vibrated. A linearly (circularly) polarized wave with an amplitude of $y \approx A \sin(\omega t)$ ($\omega \approx 208$ GHz and $A \approx 0.3–2.1$ nm) was generated by periodic oscillations of atoms close to one end of the CNT. During the simulations, performed at $T = 300$ K, a small Langevin damping coefficient of 0.01 ps^{-1} was applied to the whole system except the two CNT ends, where a damping coefficient of 10 ps^{-1} was used to absorb the phonon waves. It should be noted (inset) that after the wave passes around the droplet its amplitude becomes much smaller, signaling a large momentum transfer to the nanodroplet.

As shown in Figure 24, the translational velocities v of the droplets with $N_w = 10^3$ and 10^4 waters initially increase approximately quadratically with the wave amplitude, A. The larger droplet is about an order of magnitude slower, due to an order of magnitude larger mass (similar momentum) and larger friction with the CNT. When the droplet was dragged with circularly polarized waves, its translation was accompanied by rotation, as seen in the experiment in Figure 23. Moreover, nanodroplets surfing on circularly polarized waves of larger amplitudes easily became detached from the CNTs. These studies demonstrate that coherent mechanical vibrations of various nanostructure modes are a promising tool in material delivery on the nanoscale.

4.3. Chemically Tunable Nanoscale Liquid Propellers

In principle, molecules can also be dragged when CNTs, possibly after modification, are rotated in a suitable way. It was shown by MD simulations that molecular blades covalently attached to CNTs[256] can drag molecules in solutions onto their surfaces when the nanotubes are rotated by an external torque.[257] The torque might be delivered by chemical means through natural or synthetic molecular motors.[11−15] As shown in Figure 25, the bulk propeller (left) can pump liquid along the tube z-axis by two blades formed by pyrene molecules, attached to the opposite sides of the (8,0) CNT and tilted with respect to its axis. The surface propeller (right) pumps water orthogonal to the tube axis by four larger blades aligned straight along the axis. With real advances in synthetic chemistry, these systems could be prepared by cyclic addition reactions.[258]

The propeller blades were tested in two different chemical designs. In the "hydrophobic" propeller, the charges of the hydrogen atoms at the tips of the pyrene blades were set at 0.12 e, and those of the nearest aromatic carbon atoms at −0.12 e. In the "hydrophilic" propeller, these charges were chosen to be 0.30 e and −0.30 e, respectively. The propellers were embedded inside hydrophobic and hydrophilic solvents, fixed against translation, and rotated by a torque of T. In the simulations, the long-range electrostatic forces were computed by the particle-mesh Ewald method[130] in a periodic box 2.5 × 2.5 × 4.4 nm. Langevin dynamics[131] was used with a small damping coefficient of 0.01 ps^{-1} (time step of 1 fs).[132]

In Figure 26, we can see the temperature dependence of the rotation (up) and pumping (down) rates of the bulk hydrophobic and hydrophilic propellers obtained in the (hydrophobic) dichloromethane (DCM) and water solvents. The results were calculated by averaging the data over a trajectory with ∼50 rotations for an applied torque of $T = 0.2$ nN nm. As the system is heated above the (normal) freezing points of the solvents, $T_f^{DCM} = 175$ K and $T_f^{water} = 273$ K, the rotation rates grow, as a results of the smaller solvent viscosities. The hydrophilic propeller rotates slower, because

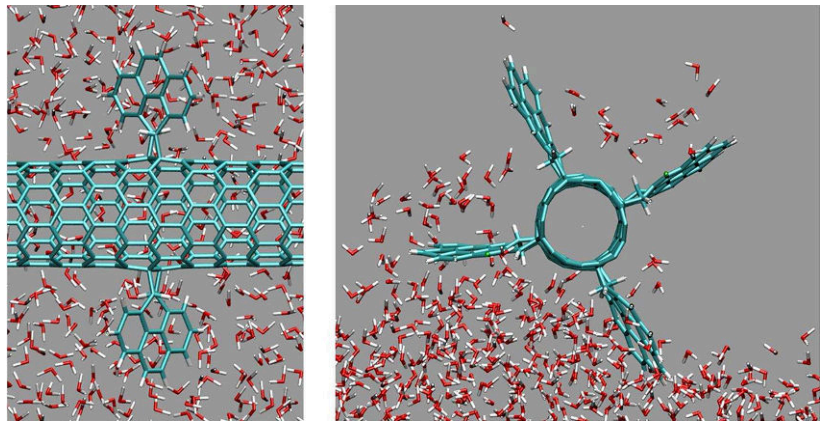


Figure 25. The bulk (left) and surface (right) water propellers that pump water along the tube axis and orthogonal to it, respectively. Both systems are based on the (8,0) CNTs and have covalently attached aromatic (hydrophobic) blades. Water is partly removed from the front of the diagram to facilitate view of the details. Reproduced with permission from ref 257. Copyright 2007 American Physical Society.

dx.doi.org/10.1021/cr200244h | Chem. Rev. 2013, 113, 3372−3390

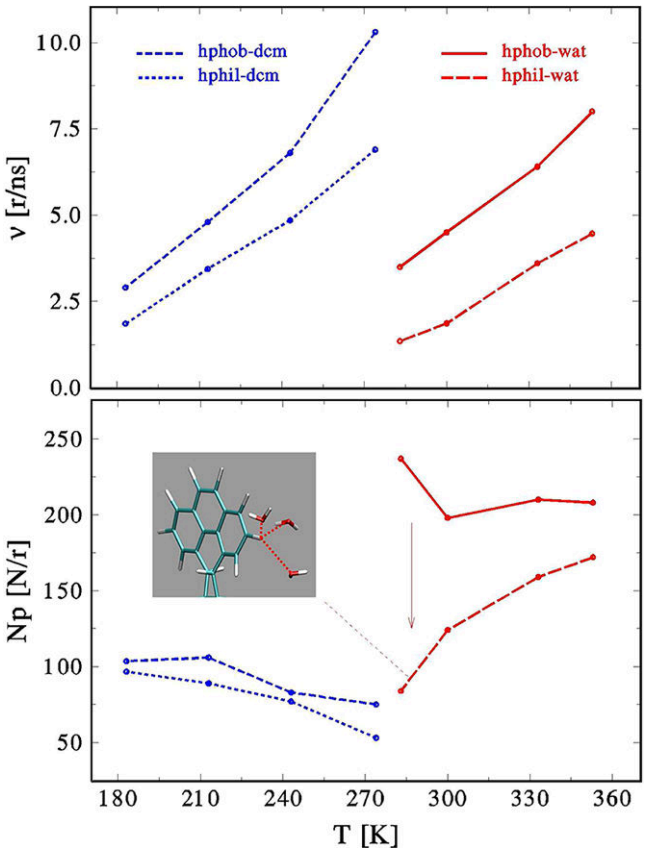


Figure 26. (up) The rotation rates (round/ns) of the bulk hydrophobic ("phob") and hydrophilic ("phil") propellers in water and DCM solvents as a function of temperature. (bottom) The pumping rates (molecules/round) of these propellers. (inset) Formation of hydrogen bonds between the hydrophilic blades and water can dramatically reduce the pumping rate. Reproduced with permission from ref 257. Copyright 2007 American Physical Society.

its polar blades interact more strongly with both solvents. A substantially slower rotation occurs in water, which forms hydrogen bonds with the polar blades[259] (see inset in Figure 26 (bottom)).

The pumping rates vary more than the rotation rates. In DCM, the rates are similar for both hydrophilic and hydrophobic propellers. In contrast, the pumping rates are very different in water, which is pumped a lot by the hydrophobic propeller, but very little by the hydrophilic propeller. This effect is caused by clogging of the hydrophilic blades by the polar water molecules.[257] We have tested that the propellers might also operate in the reverse (turbine) mode, where flowing liquids rotate the attached propellers and generate torque. The power conversion is smaller in the hydrophilic-blade turbine system than in the hydrophobic system. Analogously, it was shown that chemically functionalized nanorods can roll on water when driven by light.[260] These results demonstrate that the chemical functionalization of nanoscale mechanical devices can be used to successfully control their selectivity and efficiency, and hence the range of their applications.

5. CONCLUSIONS

In this Review, we have attempted to cover the methods of atomic and molecular drag in nanotubes.

(1) We introduced molecular drag phenomena in CNTs that are based on electron−molecule Coulombic coupling. In these phenomena, ions and molecules can be dragged through CNTs and onto their surfaces by electric currents passing through them. Alternatively, electric currents can be generated in the CNTs by polar liquids and gases passing around them. In recent years, both of these sets of predicted phenomena were observed.

(2) Next, we discussed nanofluidic phenomena based on the across-the-wall molecule−molecule Coulombic coupling that allows the dragging of ions and molecules onto the surfaces and into the interiors of C and BN nanotubes. We have also briefly described other electrokinetic phenomena, such as electroosmotic and electrophoretic drag in nanotubes. Although the across-the-wall molecule−molecule Coulombic coupling has not yet been observed experimentally, there is an analogue in the correlated passage of molecules through protein channels. Some of the electrokinetic phenomena have been seen in experiments performed with nanotubes.

(3) Finally, we described the drag of atoms, molecules, and nanoparticles inside CNTs and around them by thermal/coherent phonons and by rotations of chemically functionalized CNTs. Thermal drag is a straightforward and practical phenomenon, which has been observed in nanotubes and other nanoscale systems. The realization of coherent vibrational dragging is also relatively easy.

The drag phenomena studied allow the robust manipulation of materials on the nanoscale. Potential applications could include the delivery of individual molecules, droplets, the pumping of liquids, and the propelling of nanostructures. These numerous drag phenomena also have potential applications in fluidics, robotics, chemical sensing, medicine, and many other fields.

AUTHOR INFORMATION

Corresponding Author

*E-mail: (P.K.) pkral@uic.edu, (B.W.) wangby@iccas.ac.cn.

Notes

The authors declare no competing financial interest.

Biographies



Petr Král was born in 1961 in Prague, Czechoslovakia. In 1986, he received his M.S. degree at the Czech Technical University. After a military service, he worked at the Academy of Sciences with Karel Závěta (magnetism) and at the Palacký University with Jan Peřina (quantum optics). He then joined the Department of Condensed

Matter Theory (Academy of Sciences, Prague), where he did his Ph.D. studies in the area of quantum transport theory with Bedřich Velický (1995). From 1996–97, he stayed in the Departments of Low Dimensional Structures and Dielectrics (Acad. Sci.) and at the University of Nottingham (NATO-Royal Society Fellowship) with Fred Sheard (low-D transport). From 1997–99, he was a postdoctoral at the University of Toronto with John Sipe (coherent control). From 1999–2004, he worked at the Weizmann Institute with Moshe Shapiro (coherent control and nanoscale transport). In 2004, he joined the faculty of the Department of Chemistry at the University of Illinois at Chicago, and has been there ever since. His current research is focused on simulations of nanofluidic phenomena, nanoparticle self-assembly, nanomedicines, and calculations of electronic structures and transport in nanostructures.



Boyang Wang was born in 1982 in Jiangsu, China. In 2004, he received a B.S. in Applied Chemistry from Peking University. He did his Ph.D. at the University of Illinois at Chicago with Petr Král (2009). He then went to Northwestern University for a postdoctoral position with Igal Szleifer. From 2010–12, he had a second postdoctoral stay at the Institute of Theoretical Physics at the Chinese Academy of Sciences with Yanting Wang. In 2012, he joined the faculty of the Institute of Chemistry at the Chinese Academy of Sciences. His recent research interests include proton transfer reactions in enzyme reactions.

ACKNOWLEDGMENTS

We acknowledge the generous support of the NSF CBET-0932812 grant. B.W. would like to acknowledge support from the Paaren Graduate Fellowship of the Department of Chemistry, UIC. Numerical simulations of the drag phenomena were performed on the NERSC, NCSA, and CNM supercomputer networks.

REFERENCES

(1) Schliwa, M. *Molecular Motors*; Wiley-VCH Verlag, GmbH & Co.: New York, 2003.
(2) Vale, R. D.; Milligan, R. A. *Science* **2000**, *288*, 88.
(3) Berg, J. S.; Powell, B. C.; Cheney, R. E. *Mol. Biol. Cell* **2001**, *12*, 780.
(4) Carter, A. P.; Garbarino, J. E.; Wilson-Kubalek, E. M.; Shipley, W. E.; Cho, C.; Milligan, R. A.; Vale, R. D.; Gibbons, I. R. *Science* **2008**, *322*, 1691.
(5) Atsumi, T.; Mccartert, L.; Imae, Y. *Nature* **1992**, *355*, 182.
(6) Soong, R. K.; Bachand, G. D.; Neves, H. P.; Olkhovets, A. G.; Craighead, H. G.; Montemagno, C. D. *Science* **2000**, *290*, 1555.
(7) Brunner, C.; Wahnes, C.; Vogel, V. *Lab Chip* **2007**, *7*, 1263.
(8) Goel, A.; Vogel, V. *Nat. Nanotechnol.* **2008**, *3*, 465.
(9) Kay, E. R.; Leigh, D. A.; Zerbetto, F. *Angew. Chem.* **2006**, *46*, 72.
(10) Coskun, A.; Banaszak, M.; Astumian, R. D.; Stoddart, J. F.; Grzybowski, B. A. *Chem. Soc. Rev.* **2012**, *41*, 19.
(11) Vacek, J.; Michl, J. *Proc. Natl. Acad. Sci. U.S.A.* **2001**, *98*, 5481.
(12) Kottas, G. S.; Clarke, L. I.; Horinek, D.; Michl, J. *Chem. Rev.* **2005**, *105*, 1281.
(13) Gimzewski, J. K.; Joachim, C.; Schlittler, R. R.; Langlais, V.; Tang, H.; Johannsen, I. *Science* **1998**, *281*, 531.
(14) Kelly, T. R.; Cai, X.; Damkaci, F.; Panicker, S. B.; Tu, B.; Bushell, S. M.; Cornella, I.; Piggott, M. J.; Salives, R.; Cavero, M.; Zhao, Y.; Jasmin, S. *J. Am. Chem. Soc.* **2007**, *129*, 376.
(15) Král, P.; Vuković, L.; Patra, N.; Wang, B.; Sint, K.; Titov, A. *J. Nanosci. Lett.* **2011**, *1*, 128.
(16) Koumura, N.; Zijlstra, R. W. J.; van Delden, R. A.; Harada, N.; Feringa, B. L. *Nature* **1999**, *401*, 152.
(17) Morin, J.-F.; Shirai, Y.; Tour, J. M. *Org. Lett.* **2006**, *8*, 1713.
(18) Shirai, Y.; Osgood, A. J.; Zhao, Y.; Kelly, K. F.; Tour, J. M. *Nano Lett.* **2005**, *5*, 2330.
(19) Grill, L.; Rieder, K. H.; Moresco, F.; Rapenne, G.; Stojkovic, S.; Bouju, X.; Joachim, C. *Nat. Nanotechnol.* **2007**, *2*, 95.
(20) Král, P. *Chem. Phys. Lett.* **2003**, *382*, 399.
(21) Nam, K. T.; Kim, D. W.; Yoo, P. J.; Chiang, C. Y.; Meethong, N.; Hammond, P. T.; Chiang, Y. M.; Belcher, A. M. *Science* **2006**, *312*, 885.
(22) Iijima, S. *Nature* **1991**, *354*, 56.
(23) Dresselhaus, M. S.; Dresselhaus, G.; Eklund, P. C. *Science of Fullerenes and Carbon Nanotubes*; Academic Press Inc.: San Diego, CA, 1996.
(24) Chico, L.; Crespi, V. H.; Benedict, L. X.; Louie, S. G.; Cohen, M. L. *Phys. Rev. Lett.* **1996**, *76*, 971.
(25) Collins, P. G.; Zettl, A.; Bando, H.; Thess, A.; Smalley, R. E. *Science* **1997**, *278*, 100.
(26) Bachtold, A.; Fuhrer, M. S.; Plyasunov, S.; Forero, M.; Anderson, E. H.; Zettl, A.; McEuen, P. L. *Phys. Rev. Lett.* **2000**, *84*, 6082.
(27) Chen, J.; Hamon, M. A.; Hu, H.; Chen, Y.; Rao, A. M.; Eklund, P. C.; Haddon, R. C. *Science* **1998**, *282*, 95.
(28) Martel, R.; Schmidt, T.; Shea, H. R.; Hertel, T.; Avouris, P. *Appl. Phys. Lett.* **1998**, *73*, 2447.
(29) Baughman, R. H.; Cui, C.; Zakhidov, A. A.; Iqbal, Z.; Barisci, J. N.; Spinks, G. M.; Wallace, G. G.; Mazzoldi, A.; De Rossi, D.; Rinzler, A. G.; Jaschinski, O.; Roth, S.; Kertesz, M. *Science* **1999**, *284*, 1340.
(30) Blasé, X.; Rubio, A.; Louie, S. G.; Cohen, M. L. *Europhys. Lett.* **1994**, *28*, 335.
(31) Wong Shi Kam, N.; Jessop, T. C.; Wender, P. A.; Dai, H. *J. Am. Chem. Soc.* **2004**, *126*, 6850.
(32) Caruthers, S. D.; Wickline, S. A.; Lanza, G. M. *Curr. Opin. Biotechnol.* **2007**, *18*, 26.
(33) Cummings, J.; Zettl, A. *Science* **2000**, *289*, 602.
(34) Saito, R.; Fujita, M.; Dresselhaus, G.; Dresselhaus, M. S. *Appl. Phys. Lett.* **1992**, *60*, 2204.
(35) Zheng, M.; Jagota, A.; Strano, M. S.; Santos, A. P.; Barone, P.; Chou, S. G.; Diner, B. A.; Dresselhaus, M. S.; Mclean, R. S.; Onoa, G. B.; Samsonidze, G. G.; Semke, E. D.; Usrey, M.; Walls, D. J. *Science* **2003**, *302*, 1545.
(36) Wang, B.; Král, P.; Thanopulos, I. *Nano Lett.* **2006**, *6*, 1918.
(37) Banerjee, S.; Hemraj-Benny, T.; Wong, S. S. *Adv. Mater.* **2005**, *17*, 17.
(38) Tang, C. C.; Bando, Y. *Appl. Phys. Lett.* **2003**, *83*, 659.
(39) Chen, Y.; Zou, J.; Campbell, S. J.; Caer, G. L. *Appl. Phys. Lett.* **2004**, *84*, 2430.
(40) Král, P.; Mele, E. J.; Tománek, D. *Phys. Rev. Lett.* **2000**, *85*, 1512.
(41) Sai, N.; Mele, E. J. *Phys. Rev. B* **2003**, *68*, 241405.
(42) Ajayan, P. M.; Ebbesen, T. W.; Ichihashi, T.; Iijima, S.; Tanigaki, K.; Hiura, H. *Nature* **1993**, *362*, 522.
(43) Guerret-Piécourt, C.; Le Bouar, Y.; Lolseau, A.; Pascard, H. *Nature* **1994**, *372*, 761.
(44) Lago, R. M.; Tsang, S. C.; Lu, K. L.; Chen, Y. K.; Green, M. L. H. *J. Chem. Soc., Chem. Commun.* **1995**, 1355.
(45) Chu, A.; Cook, J.; Heesom, R. J. R.; Hutchison, J. L.; Green, M. L. H.; Sloan, J. *Chem. Mater.* **1996**, *8*, 2751.

(46) Sloan, J.; Hammer, J.; Zwiefka-Sibley, M.; Green, M. L. H. *Chem. Commun.* **1998**, 347.
(47) Shimoda, H.; Gao, B.; Tang, X. P.; Kleinhammes, A.; Fleming, L.; Wu, Y.; Zhou, O. *Phys. Rev. Lett.* **2002**, *88*, 015502.
(48) Hornbaker, D. J.; Kahng, S. J.; Misra, S.; Smith, B. W.; Johnson, A. T.; Mele, E. J.; Luzzi, D. E.; Yazdani, A. *Science* **2002**, *295*, 828.
(49) Smith, B. W.; Monthioux, M.; Luzzi, D. E. *Chem. Phys. Lett.* **1999**, *315*, 31.
(50) Kwon, Y. K.; Tománek, D.; Iijima, S. *Phys. Rev. Lett.* **1999**, *82*, 1470.
(51) Somada, H.; Hirahara, K.; Akita, S.; Nakayama, Y. *Nano Lett.* **2009**, *9*, 62.
(52) Král, P.; Tománek, D. *Phys. Rev. Lett.* **1999**, *82*, 5373.
(53) Pines, D. *Elementary Excitations in Solids*; W. A. Benjamin, Inc.: New York−Amsterdam, 1963.
(54) Gramila, T. J.; Eisenstein, J. P.; MacDonald, A. H.; Pfeiffer, L. N.; West, K. W. *Phys. Rev. Lett.* **1991**, *66*, 1216.
(55) Wingreen, N. S.; Jauho, A. P.; Meir, Y. *Phys. Rev. B* **1993**, *48*, 8487.
(56) Lunde, A. M.; Jauho, A. P. *Semicond. Sci. Technol.* **2004**, *19*, S433.
(57) Bonsager, M. C.; Flensberg, K.; Hu, B. Y. K.; MacDonald, A. H. *Phys. Rev. B* **1998**, *57*, 7085.
(58) Astumian, D. *Science* **1997**, *276*, 917.
(59) Sorbello, R. S. *Phys. Rev. B* **1989**, *39*, 4984.
(60) Kandel, D.; Kaxiras, E. *Phys. Rev. Lett.* **1996**, *76*, 1114.
(61) Lodder, A.; Dekker, J. P. *Stress Induced Phenomena in Metalliation in AIP Conf. Proc. No. 418*; AIP: New York, 1998.
(62) Atanasov, R.; Haché, A.; Hughes, L. P.; van Driel, H. M.; Sipe, J. E. *Phys. Rev. Lett.* **1996**, *76*, 1703.
(63) Deyirmenjian, V. B.; Sipe, J. E. *Phys. Rev. Lett.* **1999**, *82*, 4942.
(64) Haché, A.; Kostoulas, Y.; Atanasov, R.; Hughes, J. L. P.; Sipe, J. E.; van Driel, H. M. *Phys. Rev. Lett.* **1997**, *78*, 306.
(65) Bhat, R. D. R.; Sipe, J. E. *Phys. Rev. Lett.* **2000**, *85*, 5432.
(66) Král, P.; Sipe, J. *Phys. Rev. B* **2000**, *61*, 5381.
(67) Newson, R. W.; Ménard, J. M.; Sames, C.; Betz, M.; van Driel, H. M. *Nano Lett.* **2008**, *8*, 1586.
(68) Mele, E. J.; Král, P.; Tománek, D. *Phys. Rev. B* **2000**, *61*, 7669.
(69) Wildoer, J. W. G.; Venema, L. C.; Rinzler, A. G.; Smalley, R. E.; Dekker, C. *Nature* **1998**, *391*, 59.
(70) Kwon, Y. K.; Saito, S.; Tománek, D. *Phys. Rev. B* **1998**, *58*, R13314.
(71) Regan, B. C.; Aloni, S.; Ritchie, R. O.; Dahmen, U.; Zettl, A. *Nature* **2004**, *428*, 924.
(72) Regan, B. C.; Aloni, S.; Jensen, K.; Zettl, A. *Appl. Phys. Lett.* **2005**, *86*, 123119.
(73) Ribeiro, F. J.; Neaton, J. B.; Louie, S. G.; Cohen, M. L. *Phys. Rev. B* **2005**, *72*, 075302.
(74) Regan, B. C.; Aloni, S.; Jensen, K.; Ritchie, R. O.; Zettl, A. *Nano Lett.* **2005**, *5*, 1730.
(75) Begtrup, G. E.; Gannett, W.; Yuzvinsky, T. D.; Crespi, V. H.; Zettl, A. *Nano Lett.* **2009**, *9*, 1835.
(76) Svensson, K.; Olin, H.; Olsson, E. *Phys. Rev. Lett.* **2004**, *93*, 145901.
(77) Dong, L.; Tao, X.; Zhang, L.; Zhang, X.; Nelson, B. J. *Nano Lett.* **2007**, *7*, 58.
(78) Dong, L.; Tao, X.; Hamdi, M.; Zhang, L.; Zhang, X.; Ferreira, A.; Nelson, B. J. *Nano Lett.* **2009**, *9*, 210.
(79) Costa, P. M. F. J.; Golberg, D.; Mitome, M.; Hampel, S.; Leonhardt, A.; Buchner, B.; Bando, Y. *Nano Lett.* **2008**, *8*, 3120.
(80) Chen, J. Y.; Kutana, A.; Collier, C. P.; Giapis, K. P. *Science* **2005**, *310*, 1480.
(81) Warner, J. H.; Ito, Y.; Rummeli, M. H.; Buchner, B.; Shinohara, H.; Briggs, G. A. D. *ACS Nano* **2009**, *3*, 3037.
(82) Novoselov, K. S.; Geim, A. K.; Morozov, S. V.; Jiang, D.; Zhang, Y.; Dubonos, S. V.; Grigorieva, I. V.; Firsov, A. A. *Science* **2004**, *306*, 666.
(83) Palacios, J. J.; Fernández-Rossier, J.; Brey, L. *Phys. Rev. B* **2008**, *77*, 195428.
(84) Balog, R.; Jorgensen, B.; Nilsson, L.; Andersen, M.; Rienks, E.; Bianchi, M.; Fanetti, M.; Laegsgaard, E.; Baraldi, A.; Lizzit, S.; Sljivancanin, Z.; Besenbacher, F.; Hammer, B.; Pedersen, T. G.; Hofmann, P.; Hornekaer, L. *Nat. Mater.* **2010**, *9*, 315.
(85) Cervantes-Sodi, F.; Csanyi, G.; Piscanec, S.; Ferrari, A. C. *Phys. Rev. B* **2008**, *77*, 165427.
(86) Moser, J.; Barreiro, A.; Bachtold, A. *Appl. Phys. Lett.* **2007**, *91*, 163513.
(87) Dan, Y.; Lu, Y.; Kybert, N. J.; Luo, Z.; Johnson, A. T. C. *Nano Lett.* **2009**, *9*, 1472.
(88) Barreiro, A.; Rurali, R.; Hernández, E. R.; Bachtold, A. *Small* **2011**, *7*, 775.
(89) Král, P.; Shapiro, M. *Phys. Rev. Lett.* **2001**, *86*, 131.
(90) Ghosh, S.; Sood, A. K.; Kumar, N. *Science* **2003**, *299*, 1042.
(91) Liu, J.; Dai, L.; Baur, J. W. *J. Appl. Phys.* **2007**, *101*, 064312.
(92) Persson, B. N. J.; Tartaglino, U.; Tosatti, E.; Ueba, H. *Phys. Rev. B* **2004**, *69*, 235410.
(93) Granger, B.; Král, P.; Sadeghpour, H. R.; Shapiro, M. *Phys. Rev. Lett.* **2002**, *89*, 135506.
(94) Zhao, Y.; Song, L.; Deng, K.; Liu, Z.; Zhang, Z. X.; Yang, Y.; Wang, C.; Yang, H.; Jin, A.; Luo, Q.; Gu, C.; Xie, S.; Sun, L. *Adv. Mater.* **2008**, *20*, 1772.
(95) Liu, Z.; Zheng, K.; Hu, L.; Liu, J.; Qiu, C.; Zhou, H.; Huang, H.; Yang, H.; Li, M.; Gu, C.; Xie, S.; Xie, S.; Qiao, L.; Sun, L. *Adv. Mater.* **2008**, *20*, 1772.
(96) Barnard, R. D. *Thermoelectricity in Metals and Alloys*; Taylor and Francis: London, 1972.
(97) Romero, H. E.; Bolton, K.; Rosen, A.; Eklund, P. C. *Science* **2005**, *307*, 89.
(98) Bourlon, B.; Wong, J.; Miko, C.; Forro, L.; Bockrath, M. *Nat. Nanotechnol.* **2007**, *2*, 104.
(99) Sood, A. K.; Ghosh, S. *Phys. Rev. Lett.* **2004**, *93*, 086601.
(100) Landau, L. D.; Lifshitz, E. M. *Fluid Mechanics*, 2nd ed.; Heinemann: London, 1998.
(101) Hummer, G.; Rasaiah, J. C.; Noworyta, J. P. *Nature* **2001**, *414*, 188.
(102) Skoulidas, A. I.; Ackerman, D. M.; Johnson, J. K.; Sholl, D. S. *Phys. Rev. Lett.* **2002**, *89*, 185901.
(103) Holt, J. K.; Park, H. G.; Wang, Y.; Stadermann, M.; Artyukhin, A. B.; Grigoropoulos, C. P.; Noy, A.; Bakajin, O. *Science* **2006**, *312*, 1034.
(104) Majumder, M.; Chopra, N.; Andrews, R.; Hinds, B. J. *Nature* **2005**, *438*, 44.
(105) Wang, Z.; Ci, L.; Chen, L.; Nayak, S.; Ajayan, P. M.; Koratkar, N. *Nano Lett.* **2007**, *7*, 697.
(106) Zhou, J. J.; Noca, F.; Gharib, M. *Nanotechnology* **2006**, *17*, 4845.
(107) Whitby, M.; Quirke, N. *Nat. Nanotechnol.* **2007**, *2*, 87.
(108) Joseph, S.; Aluru, N. R. *Nano Lett.* **2008**, *8*, 452.
(109) Waghe, A.; Rasaiah, J. C.; Hummer, G. *J. Chem. Phys.* **2002**, *117*, 10789.
(110) Joseph, S.; Aluru, N. R. *Phys. Rev. Lett.* **2008**, *101*, 064502.
(111) Won, C. Y.; Aluru, N. R. *J. Am. Chem. Soc.* **2007**, *129*, 2748.
(112) Won, C. Y.; Aluru, N. R. *J. Phys. Chem. C* **2008**, *112*, 1812.
(113) Majumder, M.; Chopra, N.; Hinds, B. J. *J. Am. Chem. Soc.* **2005**, *127*, 9062.
(114) Li, J. Y.; Gong, X. J.; Lu, H. J.; Li, D.; Fang, H. P.; Zhou, R. H. *Proc. Natl. Acad. Sci. U.S.A.* **2007**, *104*, 3687.
(115) Sint, K.; Wang, B.; Král, P. *J. Am. Chem. Soc.* **2008**, *130*, 16448.
(116) Jiang, D. E.; Cooper, V. R.; Dai, S. *Nano Lett.* **2009**, *9*, 4019.
(117) Li, Y.; Zhou, Z.; Shen, P.; Chen, Z. *Chem. Commun.* **2010**, *46*, 3672.
(118) Suk, M. E.; Aluru, N. R. *J. Phys. Chem. Lett.* **2010**, *1*, 1590.
(119) Garaj, S.; Hubbard, W.; Reina, A.; Kong, J.; Branton, D.; Golovchenko, J. A. *Nature* **2010**, *467*, 190.
(120) Merchant, C. A.; Healy, K.; Wanunu, M.; Ray, V.; Peterman, N.; Bartel, J.; Fischbein, M. D.; Venta, K.; Luo, Z.; Johnson, A. T. C.; Drndić, M. *Nano Lett.* **2010**, *10*, 2915.

(121) Schneider, G. F.; Kowalczyk, S. W.; Calado, V. E.; Pandraud, G.; Zandbergen, H. W.; Vandersypen, L. M. K.; Dekker, C. *Nano Lett.* **2010**, *10*, 3163.
(122) Nelson, T.; Zhang, B.; Prezhdo, O. V. *Nano Lett.* **2010**, *10*, 3237.
(123) Wang, B.; Král, P. *J. Am. Chem. Soc.* **2006**, *128*, 15984.
(124) Wang, B.; Král, P. *Phys. Rev. Lett.* **2008**, *101*, 046103.
(125) Xiu, P.; Zhou, B.; Qi, W.; Lu, H.; Tu, Y.; Fang, H. *J. Am. Chem. Soc.* **2009**, *131*, 2840.
(126) Frisch, M. J.; Trucks, G. W.; Schlegel, H. B.; Scuseria, G. E.; Robb, M. A.; Cheeseman, J. R.; Montgomery, J. A., Jr.; Vreven, T.; Kudin, K. N.; Burant, J. C.; Millam, J. M.; Iyengar, S. S.; Tomasi, J.; Barone, V.; Mennucci, B.; Cossi, M.; Scalmani, G.; Rega, N.; Petersson, G. A.; Nakatsuji, H.; Hada, M.; Ehara, M.; Toyota, K.; Fukuda, R.; Hasegawa, J.; Ishida, M.; Nakajima, T.; Honda, Y.; Kitao, O.; Nakai, H.; Klene, M.; Li, X.; Knox, J. E.; Hratchian, H. P.; Cross, J. B.; Bakken, V.; Adamo, C.; Jaramillo, J.; Gomperts, R.; Stratmann, R. E.; Yazyev, O.; Austin, A. J.; Cammi, R.; Pomelli, C.; Ochterski, J. W.; Ayala, P. Y.; Morokuma, K.; Voth, G. A.; Salvador, P.; Dannenberg, J. J.; Zakrzewski, V. G.; Dapprich, S.; Daniels, A. D.; Strain, M. C.; Farkas, O.; Malick, D. K.; Rabuck, A. D.; Raghavachari, K.; Foresman, J. B.; Ortiz, J. V.; Cui, Q.; Baboul, A. G.; Clifford, S.; Cioslowski, J.; Stefanov, B. B.; Liu, G.; Liashenko, A.; Piskorz, P.; Komaromi, I.; Martin, R. L.; Fox, D. J.; Keith, T.; Al-Laham, M. A.; Peng, C. Y.; Nanayakkara, A.; Challacombe, M.; Gill, P. M. W.; Johnson, B.; Chen, W.; Wong, M. W.; Gonzalez, C.; Pople, J. A. *Gaussian 03*, revision C.02; Gaussian, Inc.: Wallingford, CT, 2004.
(127) MacKerell, A. D., Jr.; Banavall, N.; Foloppe, N. *Biopolymers* **2001**, *56*, 257.
(128) Phillips, J. C.; Braun, R.; Wang, W.; Gumbart, J.; Tajkhorshid, E.; Villa, E.; Chipot, C.; Skeel, R. D.; Kale, L.; Schulten, K. *J. Comput. Chem.* **2005**, *26*, 1781.
(129) Humphrey, W.; Dalke, A.; Schulten, K. *J. Mol. Graphics* **1996**, *14*, 33.
(130) Darden, T.; York, D.; Pedersen, L. *J. Chem. Phys.* **1993**, *98*, 10089.
(131) Feller, S. E.; Zhang, Y. H.; Pastor, R. W.; Brooks, B. R. *J. Chem. Phys.* **1995**, *103*, 4613.
(132) Servantie, J.; Gaspard, P. *Phys. Rev. Lett.* **2003**, *91*, 185503.
(133) Zhu, F.; Tajkhorshid, E.; Schulten, K. *Biophys. J.* **2002**, *83*, 154.
(134) Laage, D.; Hynes, J. T. *Science* **2006**, *311*, 832.
(135) McHale, G.; Newton, M. I.; Carroll, B. J. *Oil Gas Sci. Technol.* **2006**, *56*, 47.
(136) Ohtaki, H.; Radnai, T. *Chem. Rev.* **1993**, *93*, 1157.
(137) Enyashin, A. N.; Seifert, G.; Ivanovskii, A. L. *Inorg. Mater.* **2005**, *41*, 595.
(138) Kim, H. Y.; Lee, H. J.; Kang, B. H. *J. Colloid Interface Sci.* **2002**, *247*, 372.
(139) Mahadevan, L.; Pomeau, Y. *Phys. Fluids* **1999**, *11*, 2449.
(140) Brancker, A. V. *Nature* **1950**, *166*, 905.
(141) Cabria, I.; Mintmire, J. W.; White, C. T. *Phys. Rev. B* **2003**, *67*, 121406(R).
(142) Léonard, F.; Tersoff, J. *Appl. Phys. Lett.* **2002**, *81*, 4835.
(143) Vergeles, M.; Keblinski, P.; Koplik, J.; Banavar, J. R. *Phys. Rev. E* **1996**, *53*, 4852.
(144) Squires, T. M.; Quake, S. R. *Rev. Mod. Phys.* **2005**, *77*, 977.
(145) Bru, R.; Sánchez-Ferrer, A.; Garcia-Carmona, F. *Biochem. J.* **1995**, *310*, 721.
(146) van Thor, J. J.; Georgiev, G. Y.; Towrie, M.; Sage, J. T. *J. Biol. Chem.* **2005**, *280*, 33652.
(147) Wang, B.; Král, P. *Small* **2007**, *3*, 580.
(148) Baret, J. C.; Mugele, F. *Phys. Rev. Lett.* **2006**, *96*, 016106.
(149) Cevc, G., Ed. *Phospholipids Handbook*; Marcel Dekker Inc.: New York, 1993.
(150) Král, P.; Jauho, A. P. *Phys. Rev. B* **1999**, *59*, 7656.
(151) Luo, D. *MRS Bull.* **2005**, *30*, 654.
(152) Pack, D. W. *Nat. Mater.* **2004**, *3*, 133.
(153) McKnight, T. E.; Melechko, A. V.; Hensley, D. K.; Mann, D. G. J.; Griffin, G. D.; Simpson, M. L. *Nano Lett.* **2004**, *4*, 1213.
(154) Chen, X.; Kis, A.; Zettl, A.; Bertozzi, C. R. *Proc. Natl. Acad. Sci. U.S.A.* **2007**, *104*, 8218.
(155) Zheng, M.; Jagota, A.; Semke, E. D.; Diner, B. A.; Mclean, R. S.; Lustig, S. R.; Richardson, R. E.; Tassi, N. G. *Nat. Mater.* **2003**, *2*, 338.
(156) Kojima, K. K.; Fujiwara, H. *Mol. Biol. Evol.* **2003**, *20*, 351.
(157) Patra, N.; Wang, B.; Král, P. *Nano Lett.* **2009**, *9*, 3766.
(158) Wu, X. L.; Kim, J. H.; Koo, H.; Bae, S. M.; Shin, H.; Kim, M. S.; Lee, B. H.; Park, R. W.; Kim, I. S.; Choi, K.; Kwon, I. C.; Kim, K.; Lee, D. S. *Bioconjugate Chem.* **2010**, *21*, 208.
(159) Bond, P. J.; Cuthbertson, J. M.; Doel, S. S.; Sansom, M. S. *J. Am. Chem. Soc.* **2004**, *126*, 15948.
(160) Vuković, L.; Drake, S. P.; Khatib, F. A.; Madriaga, A.; Brandenburg, K. S.; Král, P.; Onyuksel, H. *J. Am. Chem. Soc.* **2011**, *133*, 13481.
(161) Patra, N.; Král, P. *J. Am. Chem. Soc.* **2011**, *133*, 6146.
(162) Moore, V. C.; Strano, M. S.; Haroz, E. H.; Hauge, R. H.; Smalley, R. E.; Schmidt, J.; Talmon, Y. *Nano Lett.* **2003**, *3*, 1379.
(163) Wu, Y.; Hudson, J. S.; Lu, Q.; Moore, J. M.; Mount, A. S.; Rao, A. M.; Alexov, E.; Ke, P. C. *J. Phys. Chem. B* **2006**, *110*, 2475.
(164) Islam, M. F.; Rojas, E.; Bergey, D. M.; Johnson, A. T.; Yodh, A. G. *Nano Lett.* **2003**, *3*, 269.
(165) O'Connell, M. J.; Boul, P.; Ericson, L. M.; Huffman, C.; Wang, Y. H.; Haroz, E.; Kuper, C.; Tour, J.; Ausman, K. D.; Smalley, R. E. *Chem. Phys. Lett.* **2001**, *342*, 265.
(166) Qiao, R.; Ke, C. P. *J. Am. Chem. Soc.* **2006**, *128*, 13656.
(167) Wallace, E. J.; Sansom, M. S. P. *Nano Lett.* **2007**, *7*, 1923.
(168) Arai, N.; Yasuoka, K.; Zeng, C. X. *J. Am. Chem. Soc.* **2008**, *128*, 7916.
(169) Melle-Franco, M.; Zerbetto, F. *Nano Lett.* **2006**, *6*, 969.
(170) Piner, R. D.; Zhu, J.; Xu, F.; Hong, S.; Mirkin, C. A. *Science* **1999**, *283*, 661.
(171) Marrink, S.; de Vries, A.; Mark, A. *J. Phys. Chem. B* **2004**, *108*, 750.
(172) Carr, R.; Weinstock, I. A.; Sivaprasadarao, A.; Müller, A.; Aksimentiev, A. *Nano Lett.* **2008**, *8*, 3916.
(173) Neri, M.; Baaden, M.; Carnevale, V.; Anselmi, C.; Maritan, A.; Carloni, P. *Biophys. J.* **2008**, *94*, 71.
(174) Wallace, E. J.; Sansom, M. S. P. *Nanotechnology* **2009**, *20*, 045101.
(175) Titov, A. V.; Král, P.; Pearson, R. *ACS Nano* **2010**, *4*, 229.
(176) Marrink, S. J.; Risselada, H. J.; Yefimov, S.; Tieleman, D. P.; de Vries, A. H. *J. Phys. Chem. B* **2007**, *111*, 7812.
(177) Shih, A. Y.; Freddolino, P. L.; Arkhipov, A.; Schulten, K. *J. Struct. Biol.* **2007**, *157*, 579.
(178) Li, B.; Li, L.; Wang, B.; Li, C. Y. *Nat. Nanotechnol.* **2009**, *4*, 358.
(179) Richard, C.; Balavoine, F.; Schultz, P.; Ebbesen, T. W.; Mioskowski, C. *Science* **2003**, *300*, 775.
(180) Schoch, R. B.; Han, J. Y.; Renaud, P. *Rev. Mod. Phys.* **2008**, *80*, 839.
(181) Daiguji, H. *Chem. Soc. Rev.* **2010**, *39*, 901.
(182) Qiao, R.; Aluru, N. R. *J. Chem. Phys.* **2003**, *118*, 4692.
(183) Travis, K. P.; Gubbins, K. E. *J. Chem. Phys.* **2000**, *112*, 1984.
(184) Borukhov, I.; Andelman, D.; Orland, H. *Electrochim. Acta* **2000**, *46*, 221.
(185) Lue, L.; Zoeller, N.; Blankschtein, D. *Langmuir* **1999**, *15*, 3726.
(186) Woelki, S.; Kohler, H. H. *Chem. Phys.* **2000**, *261*, 411.
(187) Adamczyk, Z.; Warszynski, P. *Adv. Colloid Interface Sci.* **1996**, *63*, 41.
(188) Burak, Y.; Andelman, D. *J. Chem. Phys.* **2001**, *114*, 3271.
(189) Freund, J. B. *J. Chem. Phys.* **2002**, *116*, 2194.
(190) Hunter, R. *Zeta Potential in Colloid Science: Principles and Applications*; Academic: London, 1981.
(191) Lyklema, J.; Rovillard, S.; De Coninck, J. *Langmuir* **1998**, *14*, 5659.
(192) Kirby, B. J. *Micro- and Nanoscale Fluid Mechanics: Transport in Microfluidic Devices*; Cambridge University Press: Cambridge, 2010.
(193) Xie, Y. H.; Kong, Y.; Soh, A. K.; Gao, H. J. *J. Chem. Phys.* **2007**, *127*, 225101.

(194) Yeh, I. C.; Hummer, G. *Proc. Natl. Acad. Sci. U.S.A.* **2004**, *101*, 12177.
(195) Zimmerli, U.; Koumoutsakos, P. *Biophys. J.* **2008**, *94*, 2546.
(196) Tokarz, M.; Åkerman, B.; Olofsson, J.; Joanny, J. F.; Dommersnes, P.; Orwar, O. *Proc. Natl. Acad. Sci. U.S.A.* **2005**, *102*, 9127.
(197) Fan, R.; Karnik, R.; Yue, M.; Li, D. Y.; Majumdar, A.; Yang, P. D. *Nano Lett.* **2005**, *5*, 1633.
(198) Wang, Y. C.; Stevens, A. L.; Han, J. Y. *Anal. Chem.* **2005**, *77*, 4293.
(199) Dukhin, S. S.; Derjaguin, B. V. *Electrokinetic Phenomena*; John Wiley and Sons: New York, 1974.
(200) He, J.; Lin, X.-M.; Chan, H.; Vukovic, L.; Král, P.; Jaeger, H. M. *Nano Lett.* **2011**, *11*, 2430.
(201) Haynie, D. T. *Biological Thermodynamics*; Cambridge University Press: Cambridge, 2001.
(202) Liu, H. M.; Murad, S.; Jameson, C. J. *J. Chem. Phys.* **2006**, *125*, 084713.
(203) Joseph, S.; Mashl, R. J.; Jakobsson, E.; Aluru, N. R. *Nano Lett.* **2003**, *3*, 1399.
(204) Fornasiero, F.; Park, H. G.; Holt, J. K.; Stadermann, M.; Grigoropoulos, C. P.; Noy, A.; Bakajin, O. *Proc. Natl. Acad. Sci. U.S.A.* **2008**, *105*, 17250.
(205) Corry, B. *J. Phys. Chem. B* **2008**, *112*, 1427.
(206) Hilder, T. A.; Gordon, D.; Chung, S. H. *Small* **2009**, *5*, 2870.
(207) Hilder, T. A.; Gordon, D.; Chung, S. H. *Small* **2009**, *5*, 2183.
(208) Qiao, R.; Aluru, N. R. *Nano Lett.* **2003**, *3*, 1013.
(209) Yu, M.; Funke, H. H.; Falconer, J. L.; Noble, R. D. *J. Am. Chem. Soc.* **2010**, *132*, 8285.
(210) Kalra, A.; Garde, S.; Hummer, G. *Proc. Natl. Acad. Sci. U.S.A.* **2003**, *100*, 10175.
(211) Raghunathan, A. V.; Aluru, N. R. *Phys. Rev. Lett.* **2006**, *97*, 024501.
(212) Suk, M. E.; Raghunathan, A. V.; Aluru, N. R. *Appl. Phys. Lett.* **2008**, *92*, 133120.
(213) Suk, M. E.; Aluru, N. R. *Phys. Chem. Chem. Phys.* **2009**, *11*, 8614.
(214) Rivera, J. L.; Starr, F. W. *J. Phys. Chem. C* **2010**, *114*, 3737.
(215) Qiao, R.; Georgiadis, J. G.; Aluru, N. R. *Nano Lett.* **2006**, *6*, 995.
(216) Karnik, R.; Fan, R.; Yue, M.; Li, D.; Yang, P.; Majumdar, A. *Nano Lett.* **2005**, *5*, 943.
(217) Daiguji, H.; Yang, P. D.; Majumdar, A. *Nano Lett.* **2004**, *4*, 137.
(218) Qiao, R.; Aluru, N. R. *Phys. Rev. Lett.* **2004**, *92*, 198301.
(219) Dukhin, A. S.; Dukhin, S.; Goetz, P. J. *Langmuir* **2005**, *21*, 9990.
(220) Joseph, S.; Aluru, N. R. *Langmuir* **2006**, *22*, 9041.
(221) Kim, D.; Darve, E. *J. Colloid Interface Sci.* **2009**, *330*, 194.
(222) Lyklema, J. *Fundamentals of Interface and Colloid Science*; Academic Press: New York, 1995.
(223) Cohen, A. E. *Science* **2003**, *300*, 1235.
(224) Ghosh, S.; Sood, A. K.; Ramaswamy, S.; Kumar, N. *Phys. Rev. B* **2004**, *70*, 205423.
(225) Dujardin, E.; Ebbesen, T. W.; Hiura, H.; Tanigaki, K. *Science* **1994**, *265*, 1850.
(226) Ugarte, D.; Chatelain, A.; de Heer, W. A. *Science* **1996**, *274*, 1897.
(227) Supple, S.; Quirke, N. *Phys. Rev. Lett.* **2003**, *90*, 214501.
(228) Martic, G.; Gentner, F.; Seveno, D.; Coulon, D.; De Coninck, J.; Blake, T. D. *Langmuir* **2002**, *18*, 7971.
(229) Dimitrov, D. I.; Milchev, A.; Binder, K. *Phys. Rev. Lett.* **2007**, *99*, 054501.
(230) Schebarchov, D.; Hendy, S. C. *Nano Lett.* **2008**, *8*, 2253.
(231) Schebarchov, D.; Hendy, S. C. *Phys. Rev. E* **2008**, *78*, 046309.
(232) Gao, H. J.; Kong, Y.; Cui, D. X.; Ozkan, C. S. *Nano Lett.* **2003**, *3*, 471.
(233) Gong, X.; Li, J.; Lu, H.; Wan, R.; Li, J.; Hu, J.; Fang, H. *Nat. Nanotechnol.* **2007**, *2*, 709.
(234) Wong-Ekkabut, J.; Miettinen, M. S.; Dias, C.; Karttunen, M. *Nat. Nanotechnol.* **2010**, *5*, 555.
(235) Bonthuis, D. J.; Horinek, D.; Bocquet, L.; Netz, R. R. *Phys. Rev. Lett.* **2009**, *103*, 144503.
(236) Bonthuis, D. J.; Falk, K.; Kaplan, C. N.; Horinek, D.; Berker, A. N.; Bocquet, L.; Netz, R. R. *Phys. Rev. Lett.* **2010**, *105*, 209401.
(237) Rinne, K. F.; Gekle, S.; Bonthuis, D. V.; Netz, R. R. *Nano Lett.* **2012**, *12*, 1780.
(238) Suk, M. E.; Aluru, N. R. *Phys. Rev. Lett.* **2010**, *105*, 209402.
(239) Schoen, P. A. E.; Walther, J. H.; Arcidiacono, S.; Poulikakos, D.; Koumoutsakos, P. *Nano Lett.* **2006**, *6*, 1910.
(240) Schoen, P. A. E.; Walther, J. H.; Poulikakos, D.; Koumoutsakos, P. *Appl. Phys. Lett.* **2007**, *90*, 253116.
(241) Zhao, J.; Huang, J. Q.; Wei, F.; Zhu, J. *Nano Lett.* **2010**, *10*, 4309.
(242) Zambrano, H. A.; Walther, J. H.; Jaffe, R. L. *J. Chem. Phys.* **2009**, *131*, 241104.
(243) Talbot, L.; Cheng, R. K.; Schefer, R. W.; Willis, D. R. *J. Fluid Mech.* **1980**, *101*, 737.
(244) Longhurst, M. J.; Quirke, N. *Nano Lett.* **2007**, *7*, 3324.
(245) Zambrano, H. A.; Walther, J. H.; Koumoutsakos, P.; Sbalzarini, I. F. *Nano Lett.* **2009**, *9*, 66.
(246) Shiomi, J.; Maruyama, S. *Nanotechnology* **2009**, *20*, 055708.
(247) Barreiro, A.; Rurali, R.; Hernández, E. R.; Moser, J.; Pichler, T.; Forró, L.; Bachtold, A. *Science* **2008**, *320*, 775.
(248) Insepov, Z.; Wolf, D.; Hassanein, A. *Nano Lett.* **2006**, *6*, 1893.
(249) Chen, M.; Zang, J.; Xiao, D.; Zhang, C.; Liu, F. *Nano Res.* **2009**, *2*, 938.
(250) Wang, Q. *Nano Lett.* **2009**, *9*, 245.
(251) Duan, W. H.; Wang, Q. *ACS Nano* **2010**, *4*, 2338.
(252) Xue, Q.; Xia, D.; Lv, C.; Jing, N.; Ling, C. *J. Phys. Chem. C* **2011**, *115*, 20471.
(253) Lu, H.; Nie, X.; Wu, F.; Zhou, X.; Kou, J.; Xu, Y.; Liu, Y. *J. Chem. Phys.* **2012**, *136*, 174511.
(254) Qiu, H.; Shen, R.; Guo, W. *Nano Res.* **2011**, *211*, 284.
(255) Russell, J.; Wang, B.; Král, P. *J. Phys. Chem. Lett.* **2012**, *3*, 353.
(256) Han, J.; Globus, A.; Jaffe, R.; Deardorff, G. *Nanotechnology* **1997**, *8*, 95.
(257) Wang, B.; Král, P. *Phys. Rev. Lett.* **2007**, *98*, 266102.
(258) Tasis, D.; Tagmatarchis, N.; Bianco, A.; Prato, M. *Chem. Rev.* **2006**, *106*, 1105.
(259) Silverstein, K. A. T.; Haymet, A. D. J.; Dill, K. A. *J. Am. Chem. Soc.* **2000**, *122*, 8037.
(260) Vuković, L.; Král, P. *Phys. Rev. Lett.* **2009**, *103*, 246103.